

Hamiltonian zigzag sampler got more momentum than its Markovian counterpart: Equivalence of two zigzags under a momentum refreshment limit

Akihiko Nishimura

Johns Hopkins University, Baltimore, MD, USA.

Zhenyu Zhang and Marc A. Suchard

University of California, Los Angeles, CA, USA.

Summary. Zigzag and other piecewise deterministic Markov process samplers have attracted significant interest for their non-reversibility and other appealing properties for Bayesian posterior computation. Hamiltonian Monte Carlo is another state-of-the-art sampler, exploiting fictitious momentum to guide Markov chains through complex target distributions. In this article, we uncover a remarkable connection between the zigzag sampler and a variant of Hamiltonian Monte Carlo exploiting Laplace-distributed momentum. The position and velocity component of the corresponding Hamiltonian dynamics travels along a zigzag path paralleling the Markovian zigzag process; however, the dynamics is non-Markovian as the momentum component encodes non-immediate pasts. This information is partially lost during a momentum refreshment step, in which we preserve its direction but re-sample magnitude. In the limit of increasingly frequent momentum refreshments, we prove that this Hamiltonian zigzag converges to its Markovian counterpart. This theoretical insight suggests that, by retaining full momentum information, Hamiltonian zigzag can better explore target distributions with highly correlated parameters. We corroborate this intuition by comparing performance of the two zigzag cousins on high-dimensional truncated multivariate Gaussians, including a 11,235-dimensional target arising from a Bayesian phylogenetic multivariate probit model applied to HIV virus data.

1. Introduction

Emergence of Monte Carlo methods based on continuous-time, non-reversible processes has been hailed as fundamentally new development (Fearnhead et al., 2018) and has attracted an explosion of interest in recent years (Dunson and Johndrow, 2020). The two most prominent among such algorithms are the bouncy particle sampler (Bouchard-Côté et al., 2018) and zigzag sampler (Bierkens et al., 2019a), both having roots in the computational physics literature (Peters and de With, 2012; Turitsyn et al., 2011). These algorithms draw samples from target distributions by simulating piecewise deterministic Markov processes, which move along linear trajectories with instantaneous changes in their velocities occurring at random times according to inhomogeneous Poisson processes.

One known issue with the bouncy particle sampler is its near-reducible behavior in the absence of frequent velocity refreshment (Bouchard-Côté et al., 2018; Fearnhead et al., 2018). In case of a high-dimensional i.i.d. Gaussian, Bierkens et al. (2018) show that the bouncy particle sampler's optimal performance is achieved when refreshment accounts for as much as 78% of all the velocity changes. Such frequent velocity refreshment can

lead to “random-walk behavior,” hurting computation efficiency of the sampler (Neal, 2010; Fearnhead et al., 2018; Andrieu and Livingstone, 2019).

The zigzag sampler on the other hand is provably ergodic without velocity refreshment (Bierkens et al., 2019b) and appears to have a competitive edge in high-dimensions (Bierkens et al., 2018). Much remains unknown, however, about how these samplers perform relative one another and against other classes of algorithms. Early empirical results, while informative, remain limited by their focus on low-dimensional or synthetic examples. For example, the simulated logistic regression examples in Bierkens et al. (2019a) only have 16 regression coefficients and the most complex examples of Bierkens et al. (2018) comprise 256-dimensional multi-variate Gaussians and spherically symmetric t-distributions. Generating further theoretical and empirical insight on the practical performance of these algorithms thus stands out as one of the most critical research areas (Fearnhead et al., 2018; Bierkens et al., 2019a; Dunson and Johndrow, 2020).

This article brings novel insight into the zigzag sampler’s performance by revealing its intimate connection to a version of Hamiltonian Monte Carlo (HMC), another state-of-the-art algorithm that has hitherto evolved independently. HMC exploits an auxiliary momentum variable and simulates Hamiltonian dynamics to guide exploration of the original parameter space. Initially developed for molecular dynamics simulations by Duane et al. (1987), HMC was popularized in the statistics community through the works of Neal (1996, 2010). HMC’s rise to its current prominence also owes much to the development of the no-U-turn algorithm by Hoffman and Gelman (2014) and subsequent adoption by the probabilistic programming language Stan (Carpenter et al., 2017).

We study a largely unexplored version of HMC, based on the momentum variable \mathbf{p} with its components p_i ’s having independent Laplace distributions. The corresponding Hamiltonian dynamics follows a zigzag path akin to that of the Markovian zigzag process. We thus call the resulting algorithm *zigzag HMC* and, to differentiate the dynamics underlying the two samplers, refer to them as *Hamiltonian* and *Markovian zigzag*.

The curious similarity between the two zigzags was first noted by Nishimura et al. (2020), who considered use of Laplace momentum in HMC to deal with discontinuous target distributions. However, they did not further explore the exact nature of Hamiltonian zigzag, focusing instead on how to numerically approximate its qualitative behavior.

We will show that the two zigzags are in fact equivalent under a limit of infinitely frequent momentum refreshment in Hamiltonian zigzag. We consider a partial refreshment in which p_i ’s retain their signs but have their magnitudes resampled from the exponential distributions. When this refreshment step is inserted at every $\Delta t > 0$ time interval, Hamiltonian zigzag converges in distribution to its Markovian counterpart as $\Delta t \rightarrow 0$.

This result has significant implications in the relative performance of the two zigzag algorithms. Markovian zigzag to some extent avoids random-walk behavior by retaining its direction from previous moments; the inertia induced by retaining full momentum information, however, may allow Hamiltonian zigzag to better explore the space when parameters exhibit strong dependency. The intuition is as follows. Along each coordinate, the partial derivative of the log-density depends on other coordinates and its sign can flip back and forth as the dynamics evolves. Such fluctuation leads to inconsistent guidance from the derivative, “pushing” the dynamics to one direction at one moment and to the opposite at the next. However, momentum can help each coordinate

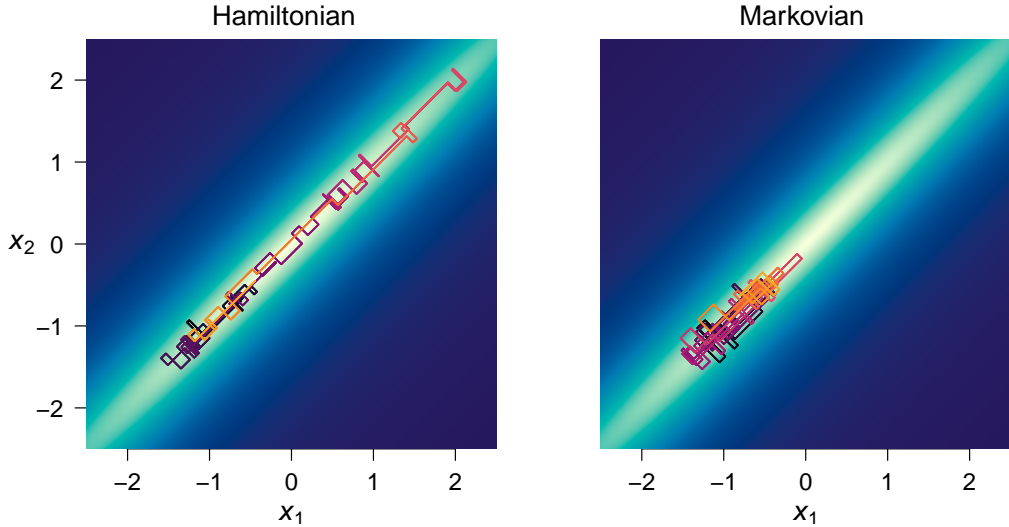


Fig. 1. Trajectories of the first two position coordinates of Hamiltonian zigzag without momentum refreshment (left) and Markovian zigzag (right). The target is a $2^{10} = 1,024$ -dimensional Gaussian, corresponding to a stationary lag-1 auto-regressive process with auto-correlation 0.99 and unit marginal variances. Both dynamics are simulated for 10^5 linear segments, starting from the same position $x_i = -1$ for all i and same random velocity. The line segment colors change from darkest to lightest as the dynamics evolve.

of the dynamics keeps traveling in an effective direction without being affected by small fluctuation in the derivative.

The advantage of having full momentum is visually illustrated in Figure 1. After comparable amounts of computation, Hamiltonian zigzag has traversed a high-density region while Markovian zigzag is still slowly diffusing away from the initial position. This difference in behavior also manifests itself in the overall distance traveled by the dynamics (Figure 2). Our observation here suggests that, with its ability to make larger transitions under comparable computational efforts, Hamiltonian zigzag constitutes a more effective transition kernel.

We empirically quantify the superior performance of Hamiltonian zigzag on a range of truncated Gaussians, a special — yet practically relevant — class of targets on which we can efficiently simulate both zigzags. One of our examples arises from a Bayesian phylogenetic multivariate probit model for studying correlation structure among binary biological traits of HIV viruses (Zhang et al., 2019). This is a real-world high-dimensional problem in which the super-linear scaling property of Markovian zigzag established by Bierkens et al. (2019a) does not hold — with the number of parameters growing proportional to that of observations, their sub-sampling and control variate techniques cannot be applied here. Our results also show that we can combine Hamiltonian zigzag with the no-U-turn algorithm to yield an effective, tuning-free, and preprocessing-free algorithm on truncated Gaussians. The truncated Gaussian sampler based on Hamiltonian zigzag is provided as a part of the Bayesian phylogenetic software BEAST (Suchard et al., 2018).

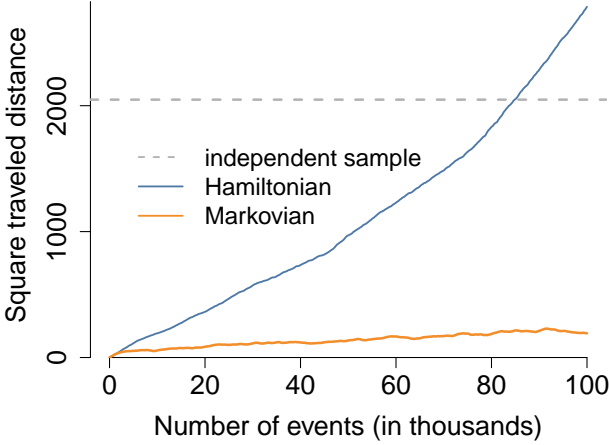


Fig. 2. Squared distance $\|x(t) - x_0\|^2$ of the two zigzag dynamics from the initial position, plotted as function of the number of velocity change events. The experimental setup is identical to that of Figure 1. The dashed line indicates the expected squared distance between the initial position and an independent sample from the target, as a benchmark of the distance traveled by an efficient transition kernel.

2. Zigzag HMC and its apparent similarity to Markovian zigzag

2.1. Hamiltonian dynamics based on Laplace momentum

In order to sample from the parameter of interest \mathbf{x} , HMC introduces an auxiliary *momentum* variable \mathbf{p} and draws from the augmented distribution $\pi(\mathbf{x}, \mathbf{p}) := \pi(\mathbf{x})\pi(\mathbf{p})$. HMC explores the augmented space by simulating Hamiltonian dynamics, whose evolution is governed by the differential equation known as *Hamilton’s equation*:

$$\frac{d\mathbf{x}}{dt} = \nabla K(\mathbf{p}), \quad \frac{d\mathbf{p}}{dt} = -\nabla U(\mathbf{x}), \quad (1)$$

where $U(\mathbf{x}) = -\log \pi(\mathbf{x})$ and $K(\mathbf{p}) = -\log \pi(\mathbf{p})$ are referred to as *potential* and *kinetic* energy. The solution of (1) preserves the target $\pi(\mathbf{x}, \mathbf{p})$ and, if it can be simulated exactly, can be deployed as a transition kernel. Such exact simulation is infeasible in most applications, but a numerical approximation by a reversible integrator constitutes a valid Metropolis-Hastings proposal (Fang et al., 2014). To this day, the original version of HMC by Duane et al. (1987) — based on Gaussian-distributed momentum and the leapfrog integrator — dominates practice (Salvatier et al., 2016; Carpenter et al., 2017).

For the purpose of dealing with discontinuous target densities, Nishimura et al. (2020) proposes the use of Laplace momentum $\pi(\mathbf{p}) \propto \exp(-\sum_i |p_i|)$ in HMC. The authors then proceed to develop a reversible integrator that qualitatively approximates the corresponding Hamiltonian dynamics, noting only in passing the similarity of its trajectories to those of Markovian zigzag. Under Laplace momentum, Hamilton’s equation becomes

$$\frac{d\mathbf{x}}{dt} = \text{sign}(\mathbf{p}), \quad \frac{d\mathbf{p}}{dt} = -\nabla U(\mathbf{x}). \quad (2)$$

Under these dynamics, the velocity $\mathbf{v} := d\mathbf{x}/dt \in \{\pm 1\}^d$ depends only on the sign of \mathbf{p} and thus remains constant except when one of the p_i ’s undergoes a sign change. This property leads to a piecewise linear trajectory as follows.

We momentarily ignore a mathematical technicality that arises from the discontinuity of the sign function in (2). Starting from the state $(\mathbf{x}(\tau), \mathbf{p}(\tau))$ with $p_i(\tau) \neq 0$ for all i

and $\mathbf{v} = \text{sign}(\mathbf{p})$, the dynamics according to (2) evolves as

$$\mathbf{x}(\tau + t) = \mathbf{x}(\tau) + t\mathbf{v}(\tau), \quad (3)$$

$$p_i(\tau + t) = p_i(\tau) - \int_0^t \partial_i U(\mathbf{x}(\tau + s)) \, ds \quad \text{for all } i, \quad (4)$$

where (3) holds as long as the signs of p_i , and hence \mathbf{v} , remain constant on $[\tau, \tau + t]$. During this time, the momentum magnitude evolves as

$$|p_i|(\tau + t) = |p_i|(\tau) - \int_0^t v_i(\tau) \partial_i U(\mathbf{x}(\tau) + s\mathbf{v}(\tau)) \, ds \quad \text{for all } i. \quad (5)$$

From (4) and (5), we see that the sign change in p_i occurs at time $\tau + t_i$ where

$$t_i = \inf_{t > 0} \left\{ |p_i(\tau)| = \int_0^t v_i(\tau) \partial_i U(\mathbf{x}(\tau) + s\mathbf{v}(\tau)) \, ds \right\}. \quad (6)$$

Let $i^* = \arg\min_i t_i$ denote the first coordinate to experience a sign change. As p_{i^*} changes its sign at time $\tau + t_{i^*}$, the velocity $\mathbf{v} = d\mathbf{x}/dt$ undergoes an instantaneous change

$$v_{i^*}(\tau + t_{i^*}) = -v_{i^*}(\tau), \quad v_j(\tau + t_{i^*}) = v_j(\tau) \quad \text{for } j \neq i^*, \quad (7)$$

and for $t \geq t_{i^*}$ the position component proceeds along a new linear path

$$\mathbf{x}(\tau + t) = \mathbf{x}(\tau + t_{i^*}) + (t - t_{i^*})\mathbf{v}(\tau + t_{i^*}) \quad (8)$$

until the next sign change event. All the while, the momentum component continues evolving according to (4). We summarize the properties (3)–(8) in the algorithmic description of Hamiltonian zigzag in Section 2.2.

Under mild conditions, which we quantify momentarily, the trajectory of $(\mathbf{x}(t), \mathbf{p}(t))$ as described satisfies the equation (2) except at the instantaneous moments of sign changes in p_i 's. For a differential equation with discontinuous right-hand side, what constitutes a solution and whether it is unique are delicate and complex questions. A study of existence and uniqueness typically starts by interpreting the equation as a differential inclusion problem (Filippov, 1988). More precisely, given a differential equation $dz/dt = \mathbf{f}(z)$ and discontinuity points of \mathbf{f} , the equality requirement is relaxed to an inclusion of the form $dz/dt \in \mathbf{F}(z)$ for a suitable set $\mathbf{F}(z)$ e.g. a convex polytope whose extreme points consist of $\lim_{z' \rightarrow z} \mathbf{f}(z')$. The theory remains incomplete, however, despite years of research effort (Fetecau et al., 2003; Khulief, 2013).

As existing theory falls short, we will directly establish an existence and uniqueness result for Hamilton's equation with Laplace momentum. For continuously differentiable U , the process (3)–(8) defines a unique trajectory consistent with (2) as long as it stays away from the sets

$$S_i = \{(\mathbf{x}, \mathbf{p}) : \partial_i U(\mathbf{x}) = 0, p_i = 0\}. \quad (9)$$

If $\partial_i U(\mathbf{x}(\tau + t_i)) \neq 0$ at the moment of sign change $p_i(\tau + t_i) = 0$, the relation (4) dictates that

$$\lim_{t \rightarrow t_i^+} \text{sign}(p_i(\tau + t)) = -\lim_{t \rightarrow t_i^-} \text{sign}(p_i(\tau + t)),$$

where t_i^+ and t_i^- indicate the right and left limit. Hence, the velocity change and subsequent evolution according to (7) and (8) define the only trajectory that satisfies Equation (2) for almost every $t \geq 0$ and whose position component is continuous in t .

In Theorem 2.1 below, we make a convenient assumption to ensure that a trajectory avoids the problematic sets (9) from almost every initial state. The theorem also establishes the time-reversibility and symplecticity of the dynamics, which together imply that Hamiltonian zigzag preserves the target distribution and thus constitutes a valid transition kernel (Neal, 2010; Fang et al., 2014).

THEOREM 2.1. *Suppose that U is twice continuously differentiable and that the sets $\{\mathbf{x} : \partial_i U(\mathbf{x}) = 0\}$ comprise smooth manifolds of dimension at most $d - 1$. Then, for all initial conditions $(\mathbf{x}(0), \mathbf{p}(0)) \in \mathbb{R}^{2d} \setminus \Omega$ away from a set Ω of measure zero, there exists a unique solution that satisfies Eq (2) at almost every $t \geq 0$ and whose position component is continuous in t . Moreover, the dynamics is time-reversible and symplectic on $\mathbb{R}^{2d} \setminus \Omega$.*

The assumption of Theorem 2.1 in particular holds for any strongly log-concave target since it would imply that $\nabla \partial_i U \neq 0$ and, by the implicit function theorem, that $\{\mathbf{x} : \partial_i U(\mathbf{x}) = 0\}$ is a manifold of dimension $d - 1$. More generally, the conclusions would hold under a weaker assumption as long as it ensures the trajectory does not come across the sets (9).

We note that, the exact nature of Hamiltonian zigzag on smooth targets being auxiliary to their work, Nishimura et al. (2020) establish corresponding results only under a piecewise constant U with piecewise linear discontinuity set. Given the incomplete theory behind discontinuous differential equations and non-smooth Hamiltonian mechanics, the above result is significant on its own and of independent interest. We defer the proof to Supplement S1, however, to keep the article's focus on the connection between Hamiltonian and Markovian zigzag and its implication on Monte Carlo simulation.

2.2. Simulation of Hamiltonian zigzag

To summarize the above discussion and elucidate its connection to Markovian zigzag, we describe the evolution of Hamiltonian zigzag in the space $(\mathbf{x}, \mathbf{v}, |\mathbf{p}|)$ as follows, where $p_i = v_i |p_i|$ for all i . Denoting $(\mathbf{x}^{(k)}, \mathbf{v}^{(k)}, |\mathbf{p}|^{(k)}) = \{\mathbf{x}(\tau^{(k)}), \mathbf{v}(\tau^{(k)}), |\mathbf{p}|(\tau^{(k)})\}$ with a given initial condition at time $\tau^{(0)}$, the position coordinate follows a piecewise linear path segmented by the event times $\tau^{(k)}$, in-between which the dynamics evolves according to

$$\begin{aligned} \mathbf{x}(\tau^{(k)} + t) &= \mathbf{x}^{(k)} + t\mathbf{v}^{(k)}, \quad \mathbf{v}(\tau^{(k)} + t) = \mathbf{v}^{(k)}, \text{ and} \\ |p_i|(\tau^{(k)} + t) &= |p_i|^{(k)} - \int_0^t v_i^{(k)} \partial_i U(\mathbf{x}^{(k)} + s\mathbf{v}^{(k)}) ds. \end{aligned}$$

The $(k + 1)$ th event occurs at time

$$\tau^{(k+1)} = \tau^{(k)} + \min_i t_i^{(k)} \quad \text{where} \quad t_i^{(k)} = \inf_{t > 0} \left\{ |p_i|^{(k)} = \int_0^t v_i^{(k)} \partial_i U(\mathbf{x}^{(k)} + s\mathbf{v}^{(k)}) ds \right\},$$

resulting in an instantaneous change in the i^* th component of velocity for $i^*(k) = \operatorname{argmin}_i t_i^{(k)}$:

$$v_{i^*}^{(k+1)} = -v_{i^*}^{(k)} \quad \text{and} \quad v_j^{(k+1)} = v_j^{(k)} \quad \text{for } j \neq i^*.$$

The position and momentum magnitude at time $\tau^{(k+1)}$ are given by

$$\begin{aligned} \mathbf{x}^{(k+1)} &= \mathbf{x}^{(k)} + (\tau^{(k+1)} - \tau^{(k)}) \mathbf{v}^{(k)} \text{ and} \\ |p_i|^{(k+1)} &= |p_i|^{(k)} - \int_0^{\tau^{(k+1)} - \tau^{(k)}} v_i^{(k)} \partial_i U(\mathbf{x}^{(k)} + s \mathbf{v}^{(k)}) \, ds. \end{aligned}$$

The dynamics then continues in the same manner for the next interval $[\tau^{(k+1)}, \tau^{(k+2)})$.

Algorithm 1 summarizes the trajectory simulation process as pseudo-code. For the moment, we do not concern ourselves with either how we would solve for t_i in Line 7 or how to evaluate the integrals in Line 13 and 17. As we demonstrate in Section 4, we can exploit the analytical solutions available under (truncated) multivariate Gaussians for a highly efficient implementation (Appendix B).

Algorithm 1 Hamiltonian zigzag trajectory simulation for $t \in [0, T]$

```

1: function HAMILTONIANZIGZAG( $\mathbf{x}, \mathbf{p}, T$ )
2:    $\tau \leftarrow 0$ 
3:    $\mathbf{v} \leftarrow \operatorname{sign}(\mathbf{p})$ 
4:   while  $\tau < T$  do
5:     for  $i = 1, \dots, d$  do
6:
7:      $t_i = \inf_{t>0} \left\{ |p_i| = \int_0^t v_i \partial_i U(\mathbf{x} + s \mathbf{v}) \, ds \right\}$ 
8:   end for
9:    $t^* \leftarrow \min_i t_i$ 
10:  if  $\tau + t^* > T$  then
11:     $\triangleright$  No further event occurred
12:     $\mathbf{x} \leftarrow \mathbf{x} + (T - \tau) \mathbf{v}$ 
13:     $\mathbf{p} \leftarrow \mathbf{p} - \int_0^{T-\tau} \nabla U(\mathbf{x} + s \mathbf{v}) \, ds.$ 
14:     $\tau \leftarrow T$ 
15:  else
16:     $\mathbf{x} \leftarrow \mathbf{x} + t^* \mathbf{v}$ 
17:     $\mathbf{p} \leftarrow \mathbf{p} - \int_0^{t^*} \nabla U(\mathbf{x} + s \mathbf{v}) \, ds.$ 
18:     $i^* \leftarrow \operatorname{argmin}_i t_i$ 
19:     $v_{i^*} \leftarrow -v_{i^*}$ 
20:     $\tau \leftarrow \tau + t^*$ 
21:  end if
22: end while
23: return  $(\mathbf{x}, \mathbf{p})$ 
24: end function

```

Algorithm 2 Markovian zigzag trajectory simulation for $t \in [0, T]$

```

1: function MARKOVIANZIGZAG( $\mathbf{x}, \mathbf{v}, T$ )
2:    $\tau \leftarrow 0$ 
3:
4:   while  $\tau < T$  do
5:     for  $i = 1, \dots, d$  do
6:        $u_i \sim \operatorname{Unif}(0, 1)$ 
7:        $t_i = \inf_{t>0} \left\{ -\log u_i = \int_0^t [v_i \partial_i U(\mathbf{x} + s \mathbf{v})]^+ \, ds \right\}$ 
8:     end for
9:      $t^* \leftarrow \min_i t_i$ 
10:    if  $\tau + t^* > T$  then
11:       $\triangleright$  No further event occurred
12:       $\mathbf{x} \leftarrow \mathbf{x} + (T - \tau) \mathbf{v}$ 
13:
14:     $\tau \leftarrow T$ 
15:  else
16:     $\mathbf{x} \leftarrow \mathbf{x} + t^* \mathbf{v}$ 
17:
18:     $i^* \leftarrow \operatorname{argmin}_i t_i$ 
19:     $v_{i^*} \leftarrow -v_{i^*}$ 
20:     $\tau \leftarrow \tau + t^*$ 
21:  end if
22: end while
23: return  $(\mathbf{x}, \mathbf{v})$ 
24: end function

```

2.3. Comparison with Markovian zigzag

The Markovian zigzag process by Bierkens et al. (2019a) follows a piecewise linear trajectory similar to Hamiltonian zigzag, but without any apparent concept of momentum. Starting from the state $(\mathbf{x}(\tau), \mathbf{v}(\tau))$ with $\mathbf{v} \in \{\pm 1\}^d$, Markovian zigzag follows a linear path

$$\mathbf{x}(\tau + t) = \mathbf{x}(\tau) + t\mathbf{v}(\tau), \quad \mathbf{v}(\tau + t) = \mathbf{v}(\tau)$$

for $t \geq 0$ until the next velocity switch event $v_i \leftarrow -v_i$ that occurs with Poisson rate

$$\lambda_i(\mathbf{x}, \mathbf{v}) = [v_i \partial_i U(\mathbf{x})]^+ := \max\{0, v_i \partial_i U(\mathbf{x})\}. \dagger \quad (10)$$

In particular, the next event time $\tau + t^*$ can be simulated by setting $t^* = \min_i t_i$ where

$$t_i = \inf_{t>0} \left\{ -\log u_i = \int_0^t [v_i(\tau) \partial_i U(\mathbf{x}(\tau) + s\mathbf{v}(\tau))]^+ ds \right\} \quad \text{for } u_i \sim \text{Unif}(0, 1). \quad (11)$$

Denoting $i^* = \operatorname{argmin}_i t_i$, at time $\tau + t^*$ the velocity undergoes an instantaneous change

$$v_{i^*}(\tau + t_{i^*}) = -v_{i^*}(\tau), \quad v_j(\tau + t_{i^*}) = v_j(\tau) \quad \text{for } j \neq i^*,$$

and for $t \geq t_{i^*}$ the position component proceeds along a new linear path

$$\mathbf{x}(\tau + t) = \mathbf{x}(\tau + t_{i^*}) + (t - t_{i^*})\mathbf{v}(\tau + t_{i^*})$$

until the next sign change event.

Algorithm 2 describes the dynamics of Markovian zigzag in pseudo-code with empty lines inserted as appropriate to facilitate comparison with the dynamics of Hamiltonian zigzag. The similarity between the two zigzags is striking. The main difference lies in Lines 6 and 7 of the algorithms, reflecting the formulae (11) and (6) for their respective velocity switch event times. First, Markovian zigzag's event time depends on the random quantity u_i . We will see in Section 3, however, that the distributional equality $-\log u_i \stackrel{d}{=} |p_i| \sim \text{Exp}(\text{scale} = 1)$ is a key element connecting the two zigzags at a deeper level.

The quantities $-\log u_i$ and $|p_i|$ being comparable, the only remaining difference between (11) and (6) is the presence and absence of the positive part operator $[\cdot]^+$ in the integrands. The presence and absence of $[\cdot]^+$ are manifestations of the fact that Markovian zigzag is memory-less while Hamiltonian zigzag transfers energy between the potential and kinetic parts and encodes this information in the form of momentum. The etiology and consequence of this difference is most easily seen in the case of a one-dimensional unimodal target $U(x)$, as visually illustrated in Figure 3. Before a velocity

† Markovian zigzag based on the rate (10) is referred to as the *canonical zigzag* by Bierkens et al. (2019a) and is the predominant version in the literature. More generally, however, any Poisson rate satisfying $\lambda_i(\mathbf{x}, \mathbf{v}) - \lambda_i(\mathbf{x}, F_i(\mathbf{v})) = v_i \partial_i U(\mathbf{x})$ can be used, where $[F_i(\mathbf{v})]_i = -v_i$ and $[F_j(\mathbf{v})]_j = v_j$ for $j \neq i$.

switch event, a zigzag trajectory from the initial position x_0 and velocity v_0 satisfies

$$\begin{aligned} \int_0^t [v_0 \partial_i U(x_0 + sv_0)]^+ ds &= \begin{cases} 0 & \text{for } 0 \leq t \leq t_{\min} \\ U(x_0 + tv_0) - U_{\min} & \text{for } t > t_{\min}, \end{cases} \\ \int_0^t v_0 \partial_i U(x_0 + sv_0) ds &= U(x_0 + tv_0) - U(x_0) \\ &= U(x_0 + tv_0) - U_{\min} - [U(x_0) - U_{\min}], \\ \text{where } t_{\min} &:= \underset{t \geq 0}{\operatorname{argmin}} U(x_0 + tv_0) \quad \text{and} \quad U_{\min} := U(x_0 + t_{\min} v_0). \end{aligned}$$

The velocity switch event formulae (11) and (6) therefore simplify to

$$\begin{aligned} t^M &= \inf_{t \geq t_{\min}} \{ -\log u \mid U(x_0 + tv_0) - U_{\min} \}, \\ t^H &= \inf_{t \geq t_{\min}} \{ U(x_0) - U_{\min} + |p_0| \mid U(x_0 + tv_0) - U_{\min} \}. \end{aligned} \quad (12)$$

From (12), we see that the Markovian event necessarily precedes the Hamiltonian one (i.e. $t^M \leq t^H$) when $|p_0| = -\log u$ and $|p(t_{\min})| = U(x_0) - U_{\min} + |p_0| \geq -\log u$.

In higher dimensions, the same reasoning applies to the relative behavior of the two zigzags along each coordinate. On average, the memory-less property as manifested by the presence of $[\cdot]^+$ in (11) causes Markovian zigzag to experience more frequent velocity switch events and travel shorter distances along each linear path. In contrast, when a coordinate of Hamiltonian zigzag is going down potential energy hills (i.e. $v_i \partial_i U(\mathbf{x}) < 0$), the decrease in potential energy causes an equivalent increase in kinetic energy and in momentum magnitude as dictated by the relation (5). Hamiltonian zigzag can then use this stored kinetic energy to continue traveling in the same direction for longer distances.

3. Markovian zigzag as infinite momentum refreshment limit of Hamiltonian zigzag

We now consider a version of Hamiltonian zigzag in which we periodically refresh the momentum by resampling their magnitudes $|p_i(\tau)| \sim \operatorname{Exp}(1)$ while keeping their signs. This process follows a zigzag path as before, but its inter-event times are now random. We see from the formula of (6) that, following a momentum magnitude refreshment at time τ , the velocity flip $v_i \leftarrow -v_i$ occurs during the interval $[\tau, \tau + \Delta t]$ if and only if

$$|p_i(\tau)| \leq \max_{0 \leq t \leq \Delta t} \left[\int_0^t v_i(\tau) \partial_i U(\mathbf{x}(\tau + s)) ds \right].$$

Provided that $\partial_i U$ is continuous and $\partial_i U(x(\tau)) \neq 0$, the sign of $\partial_i U(\mathbf{x}(\tau + s))$ stays constant on the interval $s \in [\tau, \tau + \Delta t]$ for sufficiently small Δt , so that

$$\max_{0 \leq t \leq \Delta t} \left[\int_0^t v_i(\tau) \partial_i U(\mathbf{x}(\tau + s)) ds \right] < 0 \quad \text{or} \quad = \int_0^{\Delta t} [v_i(\tau) \partial_i U(\mathbf{x}(\tau + s))]^+ ds.$$

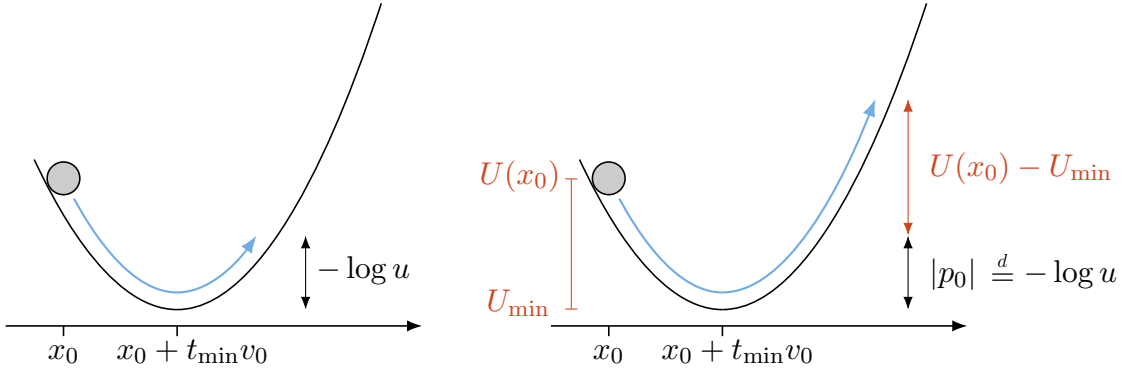


Fig. 3. Comparison of Markovian (left) and Hamiltonian (right) zigzag trajectories under the one-dimensional potential $U(x)$. Neither zigzag is affected by velocity switch events while going down the potential energy hill, i.e. while the velocity and gradient point in the opposite directions so that $v(t)\partial U(x(t)) < 0$. During this time, Hamiltonian zigzag stores up kinetic energy converted from potential energy, while Markovian zigzag remains memory-less. Once the trajectories reaches the potential energy minimum $U_{\min} := \operatorname{argmin}_{t \geq 0} U(x_0 + tv_0)$ and start going “uphill,” the accumulated momentum $|p(t_{\min})| = |p_0| + U(x_0) - U_{\min}$ keeps Hamiltonian zigzag traveling in the same direction longer than Markovian zigzag. More precisely, the last statement only holds “on average” due to randomness in the realized values of $|p_0| \stackrel{d}{=} -\log u$.

Under these conditions, the probability of the i -th velocity flip is therefore

$$\begin{aligned}
 & \mathbb{P} \left\{ |p_i(\tau)| \leq \max_{0 \leq t \leq \Delta t} \left[\int_0^t v_i(\tau) \partial_i U(\mathbf{x}(\tau + s)) \, ds \right] \right\} \\
 &= \mathbb{P} \left\{ |p_i(\tau)| \leq \int_0^{\Delta t} [v_i(\tau) \partial_i U(\mathbf{x}(\tau + s))]^+ \, ds \right\} \\
 &= 1 - \exp \left\{ - \int_0^{\Delta t} [v_i(\tau) \partial_i U(\mathbf{x}(\tau + s))]^+ \, ds \right\} \\
 &= [v_i(\tau) \partial_i U(\mathbf{x}(\tau))]^+ \Delta t + O(\Delta t^2).
 \end{aligned} \tag{13}$$

Equation (13) shows that, following the momentum magnitude refreshment, an i -th velocity switch event for Hamiltonian zigzag happens at a rate essentially identical to that of Markovian zigzag as given in (10).

Now consider resampling the momentum magnitude after every time interval of size Δt and letting $\Delta t \rightarrow 0$. Our analysis above suggests that, under this limit, the rate of coordinate-wise velocity switch events for Hamiltonian zigzag converges to $\lambda_i(\mathbf{x}, \mathbf{v}) = [v_i \partial_i U(\mathbf{x})]^+$. That is, Hamiltonian zigzag becomes *equivalent* to Markovian zigzag under the infinite momentum refreshment limit.

We now turn the above intuition into a rigorous argument. In Theorem 3.1 below, $D[0, \infty)$ denotes the space of right-continuous-with-left-limit functions from $[0, \infty)$ to $\mathbb{R}^d \times \mathbb{R}^d$ endowed with Skorokhod topology, the canonical space to study convergence of stochastic processes with jumps (Billingsley, 1999; Ethier and Kurtz, 2005). In particular, the convergence $(\mathbf{x}_{\Delta t}, \mathbf{v}_{\Delta t}) \rightarrow (\mathbf{x}, \mathbf{v})$ in this space implies the convergence of the

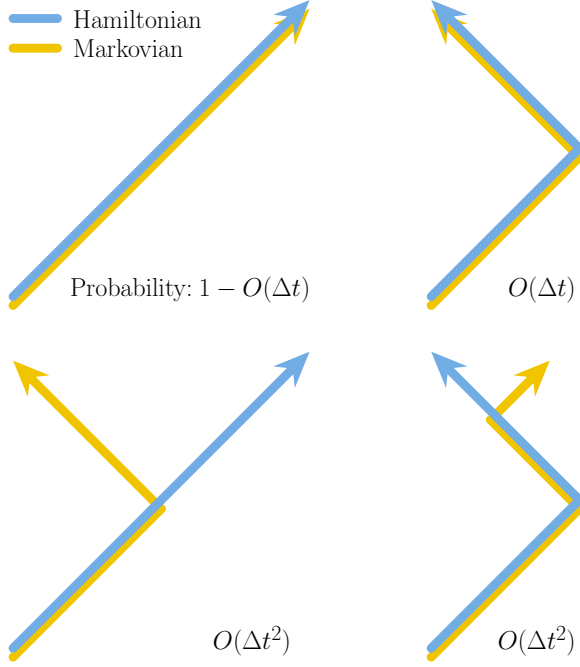


Fig. 4. Potential trajectories of the coupled Hamiltonian (blue) and Markovian (yellow) zigzag on an interval $[n\Delta t, (n+1)\Delta t]$ conditional on them being at the same state at time $n\Delta t$. With probability $1 - O(\Delta t)$ or $O(\Delta t)$, the two zigzags trace the same exact path with zero or one velocity switch event (top left and top right). The paths diverge with probability at most $O(\Delta t^2)$ (bottom left and bottom right).

ergodic average $T^{-1} \int_0^T f(\mathbf{x}_{\Delta t}(t)) dt \rightarrow T^{-1} \int_0^T f(\mathbf{x}(t)) dt$ for any continuous real-valued function f .

THEOREM 3.1. *Given an initial position $\mathbf{x}(0)$ and velocity $\mathbf{v}(0) \in \{\pm 1\}^d$, consider Hamiltonian zigzag dynamics with $p_i(0) = v_i(0)|p_i(0)|$ with $|p_i(0)| \sim \text{Exp}(1)$ and with momentum magnitude resampling at every Δt interval i.e. $|p_i(n\Delta t)| \sim \text{Exp}(1)$ for $n \in \mathbb{Z}^+$. For each Δt , let $(\mathbf{x}_{\Delta t}, \mathbf{p}_{\Delta t})$ denote the corresponding dynamics and $\mathbf{v}_{\Delta t}$ the right-continuous modification of velocity $d\mathbf{x}_{\Delta t}/dt = \text{sign}(\mathbf{p}_{\Delta t})$. Then, as $\Delta t \rightarrow 0$, the dynamics $(\mathbf{x}_{\Delta t}, \mathbf{v}_{\Delta t})$ converges weakly to the Markovian zigzag process in $D[0, \infty)$.*

In the proof to follow, we in fact establish a stronger convergence-in-probability type result (Billingsley, 1999) via explicit coupling of Hamiltonian and Markovian zigzag processes. More precisely, we construct a family of Hamiltonian zigzag $(\mathbf{x}_{\Delta t}^H, \mathbf{p}_{\Delta t}^H)$ and Markovian zigzag $(\mathbf{x}_{\Delta t}^M, \mathbf{v}_{\Delta t}^M)$ processes on the same probability space so that, for any $\epsilon > 0$ and $T > 0$,

$$\lim_{\Delta t \rightarrow 0} \mathbb{P}\{\rho_T[(\mathbf{x}_{\Delta t}^H, \mathbf{v}_{\Delta t}^H), (\mathbf{x}_{\Delta t}^M, \mathbf{v}_{\Delta t}^M)] > \epsilon\} = 0, \quad (14)$$

where $\mathbf{v}_{\Delta t}^H$ is the right-continuous modification of $\text{sign}(\mathbf{p}_{\Delta t}^H)$ and $\rho_T(\cdot, \cdot)$ is the Skorokhod metric on $[0, T]$. The distribution of Hamiltonian zigzag $(\mathbf{x}_{\Delta t}^H, \mathbf{v}_{\Delta t}^H)$ depends on Δt due to momentum magnitude refreshments, but their Markovian counterparts all have the same distribution $(\mathbf{x}_{\Delta t}^M, \mathbf{v}_{\Delta t}^M) \stackrel{d}{=} (\mathbf{x}^M, \mathbf{v}^M)$. By Theorem 3.1 of Billingsley (1999), convergence in the sense of (14) implies weak convergence $(\mathbf{x}_{\Delta t}^H, \mathbf{v}_{\Delta t}^H) \rightarrow (\mathbf{x}^M, \mathbf{v}^M)$ in $D[0, T]$ for any $T > 0$ and hence, by Theorem 16.7 of Billingsley (1999), in $D[0, \infty)$.

We couple the two zigzags by using the same random variable $u_{n,i} \sim \text{Unif}(0, 1)$ for the momentum refreshment $|p_i^H(n\Delta t)| = -\log(u_{n,i})$ and simulation of the velocity

switch event time (11) for $(\mathbf{x}_{\Delta t}^M, \mathbf{v}_{\Delta t}^M)$ on $[n\Delta t, (n+1)\Delta t]$. The critical property of our coupling is visually illustrated in Figure 4. Our construction guarantees that, given $(\mathbf{x}_{\Delta t}^H, \mathbf{v}_{\Delta t}^H)(n\Delta t) = (\mathbf{x}_{\Delta t}^M, \mathbf{v}_{\Delta t}^M)(n\Delta t)$, the probability of the two zigzag trajectories diverging on the next time interval $[n\Delta t, (n+1)\Delta t]$ is at most $O(\Delta t^2)$. Therefore, the total probability of them diverging during any of the $\lceil T/\Delta t \rceil$ intervals is $O(\Delta t)$. In other words, with probability $1 - O(\Delta t)$, the coupled zigzags $(\mathbf{x}_{\Delta t}^H, \mathbf{p}_{\Delta t}^H)$ and $(\mathbf{x}_{\Delta t}^M, \mathbf{v}_{\Delta t}^M)$ stay together during the entire $[0, T]$ interval and hence have the Skorokhod distance of zero.

PROOF. Let $\{\mathbf{u}_n = (u_{n,1}, \dots, u_{n,d})\}$ and $\{\mathbf{w}_t = (w_{t,1}, \dots, w_{t,d})\}$ for $n \in \mathbb{Z}^+ \cup \{0\}$ and $t \in (0, \infty)$ be a collection of independent $\text{Unif}(0, 1)$ random variables. We will construct Hamiltonian zigzag out of \mathbf{u}_n and additionally require \mathbf{w}_t for Markovian zigzag. We begin with the construction of Hamiltonian zigzag with momentum magnitude refreshment. Given the initial state $\mathbf{x}_{\Delta t}^H(0) = \mathbf{x}(0)$ and $\mathbf{v}_{\Delta t}^H(0) = \mathbf{v}(0)$, set $|\mathbf{p}_{\Delta t}^H(0)| = -\log(\mathbf{u}_0)$ and $\mathbf{p}_{\Delta t}^H(0) = |\mathbf{p}_{\Delta t}^H(0)|\mathbf{v}_{\Delta t}^H(0)$. For $t \in [0, \Delta t]$, let the process evolve according to the differential equation (2). At time $t = \Delta t$, resample the momentum magnitude by setting $|\mathbf{p}^H(\Delta t)| \leftarrow -\log(\mathbf{u}_1)$ and $\mathbf{p}^H(\Delta t) \leftarrow |\mathbf{p}^H(\Delta t)|\mathbf{v}_{\Delta t}^H(\Delta t)$, after which we let the process evolve again for $[\Delta t, 2\Delta t]$ according to (2). We define the rest of dynamics inductively on the intervals $[n\Delta t, (n+1)\Delta t]$ until $(n+1)\Delta t > T$, assigning

$$|\mathbf{p}_{\Delta t}^H(n\Delta t)| = -\log(\mathbf{u}_n).$$

We now turn to the construction of Markovian zigzag, first focusing on the interval $[0, \Delta t]$. Given the initial state $\mathbf{x}_{\Delta t}^M(0) = \mathbf{x}(0)$ and $\mathbf{v}_{\Delta t}^M(0) = \mathbf{v}(0)$, the process travels along a linear path with constant velocity

$$\mathbf{x}_{\Delta t}^M(t) = \mathbf{x}(0) + t\mathbf{v}(0), \quad \mathbf{v}_{\Delta t}^M(t) = \mathbf{v}(0)$$

until time Δt or the first event time $\tau_0^{(1)} = \min_i t_{0,i}^{(1)}$ where

$$t_{0,i}^{(1)} = \inf_{t>0} \left\{ |\mathbf{p}_{\Delta t,i}^H(0)| = -\log u_{0,i} \leq \int_0^t [v_i(0) \partial_i U(\mathbf{x}(0) + s\mathbf{v}(0))]^+ ds \right\}.$$

If $\tau_0^{(1)} \leq \Delta t$, the process undergoes an instantaneous velocity change at $t = \tau_0^{(1)}$:

$$v_{\Delta t,i^*}^M(\tau_0^{(1)}) = -v_{i^*}(0) \quad \text{for } i^* = \operatorname{argmin}_i t_{0,i}^{(1)}. \quad (15)$$

The process then continues for $t \geq \tau_0^{(1)}$ along a new linear path

$$\mathbf{x}_{\Delta t}^M(t) = \mathbf{x}_{\Delta t}^M(\tau_0^{(1)}) + (t - \tau_0^{(1)})\mathbf{v}_{\Delta t}^M(\tau_0^{(1)}), \quad \mathbf{v}_{\Delta t}^M(t) = \mathbf{v}_{\Delta t}^M(\tau_0^{(1)}) \quad (16)$$

until time Δt or the next event time $\tau_0^{(2)} = \tau_0^{(1)} + \min_i t_{0,i}^{(2)}$ where

$$t_{0,i}^{(2)} = \inf_{t>0} \left\{ -\log w_{\tau_0^{(1)},i} \leq \int_0^t [v_{\Delta t,i}^M(\tau_0^{(1)}) \partial_i U(\mathbf{x}_{\Delta t}^M(\tau_0^{(1)}) + s\mathbf{v}_{\Delta t}^M(\tau_0^{(1)}))]^+ ds \right\}, \quad (17)$$

undergoing instantaneous velocity change at $t = \tau_0^{(2)}$ if $\tau_0^{(2)} \leq \Delta t$:

$$v_{\Delta t,i^*}^M(\tau_0^{(2)}) = -v_{i^*}(\tau_0^{(1)}) \quad \text{for } i^* = \operatorname{argmin}_i t_{0,i}^{(2)}.$$

Continuing this construction until $\tau_0^{(k)} > \Delta t$ defines the Markovian zigzag process on $[0, \Delta t]$ with the given initial condition (Davis, 1993; Bierkens et al., 2019a).

Our construction of Markovian zigzag on $[0, \Delta t]$ so far follows the standard algorithm for simulating piecewise deterministic Markov processes, except for the fact that we couple the Markovian zigzag to its Hamiltonian counter-part via the random variable $\mathbf{u}_0 = \exp(-|\mathbf{p}_{\Delta t}^H(0)|)$. In case $\tau_0^{(1)} \leq \Delta t$, however, the evolution of $(\mathbf{x}_{\Delta t}^M(t), \mathbf{v}_{\Delta t}^M(t))$ after $t = \tau_0^{(1)}$ would have little relation to that of $(\mathbf{x}_{\Delta t}^H(t), \mathbf{v}_{\Delta t}^H(t))$. To ensure that the two processes remain closely interrelated, we “re-couple” them at every Δt interval through the shared random variable \mathbf{u}_n . More precisely, for each $n \in \mathbb{Z}^+$, we define the first potential event time on $[n\Delta t, (n+1)\Delta t]$ as $\tau_n^{(1)} = \tau_{n-1}^{(1)} + \min_i t_{n,i}^{(1)}$ where

$$\begin{aligned} t_{n,i}^{(1)} &= \inf_{t>0} \left\{ |p_{\Delta t,i}^H(n\Delta t)| = -\log u_{n,i} \right. \\ &\quad \left. \leq \int_0^t [v_{\Delta t,i}^M(n\Delta t) \partial_i U(\mathbf{x}_{\Delta t}^M(n\Delta t) + s\mathbf{v}_{\Delta t}^M(n\Delta t))]^+ ds \right\}. \end{aligned}$$

If $t_{n,i}^{(1)} < \Delta t$, the process continues for the rest of $t \in [n\Delta t, (n+1)\Delta t]$ in the same manner as it did on $[0, \Delta t]$, according to the appropriate analogues of (15), (16), and (17). The process is thus defined inductively until $(n+1)\Delta t > T$. The described procedure defines the same transition kernel on the intervals $[n\Delta t, (n+1)\Delta t]$ as on $[0, \Delta t]$. By the Markov property and Chapman-Kolmogorov equation (Davis, 1993), therefore, the process $(\mathbf{x}_{\Delta t}^M, \mathbf{v}_{\Delta t}^M)$ defines Markovian zigzag on $[0, T]$.

We now show that the coupled Hamiltonian and Markovian zigzag process follow the exact same path with high probability. Observe that

$$\begin{aligned} &\mathbb{P}\{(\mathbf{x}_{\Delta t}^H, \mathbf{v}_{\Delta t}^H) \equiv (\mathbf{x}_{\Delta t}^M, \mathbf{v}_{\Delta t}^M) \text{ on } [0, \lceil T/\Delta t \rceil \Delta t]\} \\ &= \prod_{n=0}^{\lceil T/\Delta t \rceil} \mathbb{P}\left\{ \begin{array}{l} (\mathbf{x}_{\Delta t}^H, \mathbf{v}_{\Delta t}^H) \equiv (\mathbf{x}_{\Delta t}^M, \mathbf{v}_{\Delta t}^M) \\ \text{on } [n\Delta t, (n+1)\Delta t] \end{array} \middle| \begin{array}{l} (\mathbf{x}_{\Delta t}^H, \mathbf{v}_{\Delta t}^H) \equiv (\mathbf{x}_{\Delta t}^M, \mathbf{v}_{\Delta t}^M) \text{ on } [0, n\Delta t] \end{array} \right\} \\ &= \prod_{n=0}^{\lceil T/\Delta t \rceil} \mathbb{P}\left\{ \begin{array}{l} (\mathbf{x}_{\Delta t}^H, \mathbf{v}_{\Delta t}^H) \equiv (\mathbf{x}_{\Delta t}^M, \mathbf{v}_{\Delta t}^M) \\ \text{on } [n\Delta t, (n+1)\Delta t] \end{array} \middle| (\mathbf{x}_{\Delta t}^H, \mathbf{v}_{\Delta t}^H)(n\Delta t) = (\mathbf{x}_{\Delta t}^M, \mathbf{v}_{\Delta t}^M)(n\Delta t) \right\}, \quad (18) \end{aligned}$$

where the second equality follows from the conditional independence of the processes on $[0, n\Delta t]$ and $[n\Delta t, \infty)$ by construction. Applying Lemma 3.2 to each term in (18), we have

$$\begin{aligned} \mathbb{P}\{(\mathbf{x}_{\Delta t}^H, \mathbf{v}_{\Delta t}^H) \equiv (\mathbf{x}_{\Delta t}^M, \mathbf{v}_{\Delta t}^M) \text{ on } [0, \lceil T/\Delta t \rceil \Delta t]\} &\geq (1 - C_T(\mathbf{x}(0))\Delta t^2)^{\lceil T/\Delta t \rceil} \\ &\geq 1 - C_T(\mathbf{x}(0))(T + \Delta t)\Delta t, \end{aligned} \quad (19)$$

where we can take $C_T(\mathbf{x}) = L_T(\mathbf{x})^2 d(d-1)/2 + 2 \max\{\kappa_T(\mathbf{x})d^{3/2}, L_T(\mathbf{x})d^2\}$ in terms of $L_T(\mathbf{x})$ and $\kappa_T(\mathbf{x})$ as in (20) since $\mathbf{x}_{\Delta t}^H(t)$ and $\mathbf{x}_{\Delta t}^M(t)$ stay within the L^∞ -ball B_T for all $t \in [0, T]$. We conclude from (19) that, as $\Delta t \rightarrow 0$,

$$\mathbb{P}\{\rho_T[(\mathbf{x}_{\Delta t}^H, \mathbf{v}_{\Delta t}^H), (\mathbf{x}_{\Delta t}^M, \mathbf{v}_{\Delta t}^M)] = 0\} = \mathbb{P}\{(\mathbf{x}_{\Delta t}^H, \mathbf{v}_{\Delta t}^H) \equiv (\mathbf{x}_{\Delta t}^M, \mathbf{v}_{\Delta t}^M) \text{ on } [0, T]\} \rightarrow 1. \quad \square$$

Lemma 3.2 below is used in our proof of Theorem 3.1 and is proved in Appendix A.

LEMMA 3.2. *For fixed \mathbf{x}_n and \mathbf{v}_n , we have*

$$\mathbb{P} \left\{ \begin{array}{l} (\mathbf{x}_{\Delta t}^H, \mathbf{v}_{\Delta t}^H) \equiv (\mathbf{x}_{\Delta t}^M, \mathbf{v}_{\Delta t}^M) \\ \text{on } [n\Delta t, (n+1)\Delta t] \end{array} \mid (\mathbf{x}_{\Delta t}^H, \mathbf{v}_{\Delta t}^H)(n\Delta t) = (\mathbf{x}_{\Delta t}^M, \mathbf{v}_{\Delta t}^M)(n\Delta t) = (\mathbf{x}_n, \mathbf{v}_n) \right\} \\ \geq 1 - \left(L_{\Delta t}(\mathbf{x}_n)^2 d(d-1)/2 + 2 \max\{\kappa_{\Delta t}(\mathbf{x}_n) d^{3/2}, L_{\Delta t}(\mathbf{x}_n) d^2\} \right) \Delta t^2$$

where

$$\begin{aligned} L_{\Delta t}(\mathbf{x}) &= \max \left\{ |\partial_i U(\mathbf{x}')| : 1 \leq i \leq d, \mathbf{x}' \in B_{\Delta t}(\mathbf{x}) \right\} \\ \kappa_{\Delta t}(\mathbf{x}) &= \max \left\{ \|\nabla \partial_i U(\mathbf{x}')\|_2 : 1 \leq i \leq d, \mathbf{x}' \in B_{\Delta t}(\mathbf{x}) \right\} \end{aligned} \quad (20)$$

with $\|\cdot\|_2$ denoting the ℓ^2 -norm and $B_r(\mathbf{x}) = \{\mathbf{x}' : \|\mathbf{x}' - \mathbf{x}\|_\infty < r\}$ an L^∞ -ball.

4. Simulation: two zigzags duel over truncated multivariate Gaussians

Our theoretical result of Section 3 shows Markovian zigzag as essentially equivalent to Hamiltonian zigzag with constant refreshment of momentum magnitude. As we heuristically argue in Section 1 and 2.3, the loss of full momentum information could make Markovian zigzag more liable to random-walk behavior in presence of strong dependency among parameters. We validate this intuition empirically in this section.

We have so far put aside the issue of numerically simulating zigzag trajectories in practice. The coordinate-wise integrator of Nishimura et al. (2020) provides one way to qualitatively approximate Hamiltonian zigzag. For exact simulations, however, both zigzags require computing the times of velocity switch events (Line 7 in Algorithm 1 & 2). Hamiltonian zigzag additionally requires computing the integrals of Line 13 and 17 for updating momentum. Being a Markovian process, Markovian zigzag allows the use of Poisson thinning in determining event times (Bierkens et al., 2018). This fact makes it somewhat easier to simulate Markovian zigzag, while an efficient implementation remains challenging except for a rather limited class of models (Vanetti et al., 2017).

Here we focus on sampling from a truncated multivariate Gaussian, a special yet practically relevant class of targets on which we can efficiently simulate both zigzags. Besides simple element-wise multiplications and additions, simulating each linear segment of the zigzags only requires solving d quadratic equations and extracting a column of the Gaussian precision matrix Φ (Appendix B). This in particular gives the zigzags a major potential advantage, depending on the structure of Φ , over other state-of-the-art algorithms for truncated Gaussians that require computationally expensive factorizations of Φ (Pakman and Paninski, 2014; Botev, 2017).

We compare performances of the two zigzags on a range of truncated Gaussians, consisting of both synthetic and real-data posteriors. As predicted, Hamiltonian zigzag emerges as a clear winner as dependency among parameters increases.

4.1. Zigzag-Nuts: tuning Hamiltonian zigzag via no-U-turn algorithm

Given the availability of analytical solutions in simulating zigzag trajectories, Markovian zigzag is completely tuning-free in the truncated Gaussian case. Hamiltonian zigzag requires periodic momentum refreshments $p_i \sim \text{Laplace}(\text{scale} = 1)$ for ergodicity, so

the integration time T in-between refreshments remains a user-specified input. On the other hand, being a reversible dynamics, Hamiltonian zigzag can take advantage of the no-U-turn algorithm (NUTS) of Hoffman and Gelman (2014) to automatically determine an effective integration time. This way, we only need to supply a base integration time ΔT to Hamiltonian zigzag — the no-U-turn algorithm will then identify an appropriate integration time $T = 2^k \Delta T$, where $k \geq 0$ is the height of a binary trajectory tree at which the trajectory exhibits a U-turn behavior for the first time.

With the automatic multiplicative adjustment of the total integration time, the combined Zigzag-NUTS algorithm only requires us to set ΔT as a reasonable underestimate of an optimal integration time. Based on the intuition that the integration time should be proportional to a width of the target in the least constrained direction (Neal, 2010), we choose ΔT for Zigzag-NUTS as follows. In the absence of truncation, this width of the target is proportional to $\nu_{\max}^{1/2}(\Phi^{-1}) = \nu_{\min}^{-1/2}(\Phi)$ where ν_{\max} and ν_{\min} denote the largest and smallest eigenvalues, both of which can be computed quickly via a small number of matrix-vector operations $\mathbf{w} \rightarrow \Phi^{-1}\mathbf{w}$ or $\mathbf{w} \rightarrow \Phi\mathbf{w}$ using the Lanczos algorithm (Meurant, 2006). For the standard HMC based on Gaussian momentum, an optimal integration time on multivariate Gaussian targets is $T = \pi\nu_{\min}^{-1/2}(\Phi)/2$ (Bou-Rabee and Sanz-Serna, 2018). This suggests that $\Delta T \approx \nu_{\min}^{-1/2}(\Phi)$ would be close to the upper end of reasonable base integration times. We hence propose a choice $\Delta T = \nu_{\min}^{-1/2}(\Phi)\Delta T_{\text{rel}}$ for $\Delta T_{\text{rel}} \leq 1$, where ΔT_{rel} represents a base integration time relative to the untruncated width.

In our numerical results, we find that $\Delta T_{\text{rel}} = 0.1$ works well in a broad range of problems. We observe further performance gains from a larger value, i.e. $\Delta T_{\text{rel}} > 0.1$, if the target is highly constrained. We use $\Delta T_{\text{rel}} = 0.1$ in this section for simplicity's sake, but additional numerical results are available in Supplement Section S2.

4.2. Simulation set-up and efficiency metrics

The existing empirical evaluations of Markovian zigzag rely on simple low-dimensional target distributions; consequently, there is great interest in having its performance tested on more challenging higher-dimensional problems (Dunson and Johndrow, 2020). We start from where Bierkens et al. (2018) left off — 256-dimensional correlated Gaussians (without truncation) — and first test the two zigzags on synthetic truncated Gaussians of dimension up to 4,096. We then proceed to a real-world application, comparing the performances of the two zigzags on a 11,235-dimensional truncated Gaussian posterior.

We compare the zigzags' performances using effective sample sizes (ESS), a well-established metric for quantifying efficiency of Markov chain Monte Carlo (MCMC) algorithms (Geyer, 2011). When assessing a relative performance of two MCMC algorithms, we also need to account for their per-iteration computational costs. We therefore report ESS per unit time, as is commonly done in the literature, with “time” referring to the actual time it takes for our code to run (not to be confused with the time scales of zigzag dynamics). We note, however, that relative computational speed can vary significantly from one computing environment to another due to various performance optimization strategies used by modern hardware, such as instruction-level parallelism and multi-tiered memory cache (Guntheroth, 2016; Nishimura and Suchard, 2018; Hol-

brook et al., 2020). For this reason, while ESS per time is arguably the most practically relevant metric, we consider an alternative and platform-independent performance metric in Supplement Section S3.

We run Zigzag-NUTS for 25,000 iterations on each synthetic posterior of Section 4.3. Each iteration of Zigzag-NUTS is more computationally intensive on the real-data posterior of Section 4.4, but also mixes more efficiently than on the hardest synthetic case. We hence use a shorter chain of 1,500 iterations on the real-data case. With these chain lengths, we obtain at least 100 ESS along each coordinate in all our examples.

For each Markovian zigzag simulation, we collect MCMC samples spaced at time intervals of size ΔT , the base integration time for Zigzag-NUTS. This way, we sample Markovian zigzag at least as frequently as Hamiltonian zigzag along their respective trajectories. We thus ensure a fair comparison between the two zigzags and, if any, tilt the comparison in favor of Markovian zigzag. To obtain at least 100 ESS along each coordinate, we simulate Markovian zigzag for $T = 250,000 \times \Delta T$ on each synthetic posterior and $T = 1,500 \times \Delta T$ on the real-data posterior, generating 250,000 and 1,500 samples respectively.

Note that, while both zigzags can in theory utilize entire trajectories to estimate posterior quantities of interest (Bierkens et al., 2019a; Nishimura and Dunson, 2020), such approaches are often impractical in high-dimensional settings due to memory constraints. In the 11,235-dimensional example of Section 4.4, for example, 1,500 iterations of Markovian (Hamiltonian) zigzag undergoes 1.6×10^8 (2.1×10^8) velocity switch events. Storing all these event locations would require 1.8 (2.4) TB in 64-bit double precision, while providing little practical benefit because of their high auto-correlations.

We implement both zigzags (Algorithm 3 and 4 in Appendix B) in the Java programming language as part of the Bayesian phylogenetic software BEAST, whose source code is available at https://github.com/beast-dev/beast-mcmc/tree/hmc_develop. We run each MCMC on a c5.2xlarge instance in Amazon Elastic Compute Cloud, equipped with 4 Intel Xeon Platinum 8124M processors and 16 GB of memory. For each target, we repeat the simulation 5 times with different seeds and report ESS averaged over these 5 independent replicates. ESS's are computed using the R CODA package (Plummer et al., 2006).

4.3. Synthetic posteriors: threshold model under correlated Gaussian priors

Bierkens et al. (2018) consider Gaussian targets with compound symmetric covariance

$$\text{Var}(x_i) = 1, \quad \text{Cov}(x_i, x_j) = \rho \in [0, 1] \quad \text{for } i \neq j. \quad (21)$$

Such a distribution can be interpreted as a prior induced by a model $x_i = \rho^{1/2}z + (1 - \rho)^{1/2}\epsilon_i$, with shared latent factor $z \sim \mathcal{N}(0, 1)$ and individual variations $\epsilon_i \sim \mathcal{N}(0, 1)$. We construct truncated Gaussian posteriors by assuming a threshold model

$$y_i = \mathbb{1}\{x_i > 0\} - \mathbb{1}\{x_i \leq 0\}.$$

An arbitrary thresholding would make it difficult to get any feel of the geometric structure behind the resulting truncated Gaussian posterior. For simplicity, therefore, we assume $y_i = 1$ for all i , inducing posteriors constrained to the region $\{x_i > 0\}$. We

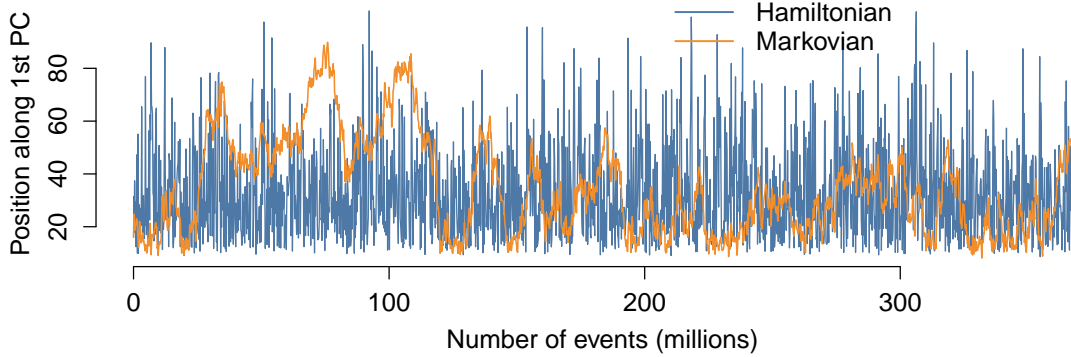


Fig. 5. Traceplot of the zigzag samples from the 1,024-dimensional compound symmetric posterior (21) with $\rho = 0.99$, projected onto the principal component $u = (1, \dots, 1)/\sqrt{d}$ via a map $x \rightarrow \langle x, u \rangle$. The horizontal axis is scaled to represent the number of velocity switch events.

investigate the effect of degree of correlation on zigzags' performance by varying the correlation coefficient, using the values $\rho = 1 - (0.1)^k$ for $k = 0, 1, 2$.

The numerical result for the compound symmetric posteriors, including the i.i.d. case $\rho = 0$, is summarized in Table 1. Since x_i are exchangeable, we calculate ESS only along the first coordinate. We also calculate ESS along the principal eigenvector of Φ^{-1} since HMC typically struggles most in sampling from the least constrained direction (Neal, 2010). Markovian zigzag face a similar challenge as evidenced by the visual comparison of the two zigzag samples projected onto the principal component (Figure 5).

As predicted, Hamiltonian zigzag demonstrates increasingly superior performance over its Markovian counterpart as the correlation increases, delivering 4.5 to 4.7-fold gains in relative ESS at $\rho = 0.9$ and 40 to 54-fold gains at $\rho = 0.99$. The efficiency gain is generally greater at the higher dimension $d = 1,024$. For the i.i.d. case, Hamiltonian zigzag seems to have no advantage. This is in a sense expected since, on an i.i.d. target, both zigzags become equivalent to running d independent one-dimensional dynamics and have no interactions among the coordinates. In other words, Hamiltonian zigzag's additional momentum plays no role when parameters are independent. Also, for a univariate Gaussian target, Markovian zigzag has been shown to induce negative auto-correlations and thus achieve sampling efficiency above that of independent Monte Carlo (Bierkens and Duncan, 2017).

The compound symmetric targets here have a particularly simple — and extreme — correlation structure; the covariance matrix can be written as $\Phi^{-1} = (1 - \rho)\mathbf{I} + \rho\mathbf{1}\mathbf{1}^\top$ for $\mathbf{1} = (1, \dots, 1)$, meaning that the probability is tightly concentrated along the principal component and is otherwise distributed symmetrically in all the other directions. This simple structure in particular allows us to manually identify an effective integration time T for Hamiltonian zigzag without too much troubles. We therefore use this synthetic example to investigate how Zigzag-NUTS perform relative to manually-tuned Hamiltonian zigzag, which we denote as "Zigzag-HMC" in Table 1.

For each of the three targets, we try $T = \nu_{\min}^{-1/2}(\Phi)T_{\text{rel}}$ with $T_{\text{rel}} = 2^{k/2}$ for $k =$

Table 1. Ess per computing time — relative to that of Markovian zigzag — under the compound symmetric posteriors. We test the algorithms under three correlation parameter values ($\rho = 0, 0.9$, and 0.99) and two varying dimensions ($d = 256$ and $1,024$). Ess are calculated along the first coordinate and along the principal eigenvector of Φ^{-1} , each shown under the labels “ x_1 ” and “PC.”

Compound symmetric	Relative Ess per time				
	$\rho = 0$		$\rho = 0.9$		$\rho = 0.99$
	x_1	PC	x_1	PC	x_1
Case: $d = 256$					
Markovian	1	1	1	1	1
Zigzag-NUTS	0.64	4.5	4.6	41	40
Zigzag-HMC ($T_{\text{rel}} = \sqrt{2}$)	5.5	46	66	180	180
Case: $d = 1,024$					
Zigzag-NUTS	0.57	4.7	4.5	54	54
Zigzag-HMC ($T_{\text{rel}} = \sqrt{2}$)	5.6	56	85	300	300

$-2, -1, 0, 1, 2$. We report the ESS’s based on $T_{\text{rel}} = 2^{1/2}$ in Table 1 as we find this choice to yield the optimal ESS in the majority of cases. We see that manually-optimized Hamiltonian zigzag delivers substantial increases in ESS compared to Zigzag-NUTS. Such efficiency gains are also observed by the authors who proposed alternative methods for tuning HMC (Wang et al., 2013; Wu et al., 2018). The results here indicate that their tuning approaches may be worthy alternatives to Zigzag-NUTS and may further increase Hamiltonian zigzag’s overall advantage over Markovian zigzag.

4.4. Posterior from phylogenetic multivariate probit model

We now consider a real-world 11,235-dimensional target from the Bayesian phylogenetic multivariate probit model of Zhang et al. (2019). For simplicity’s sake, here we describe the model with some simplifications and refer interested readers to the original work for the precise picture.

The goal of Zhang et al. (2019) is to learn correlation structure among $m = 21$ binary biological traits across $n = 535$ HIV viruses while accounting for their shared evolutionary history. Their model assumes that, conditional on the bifurcating phylogenetic tree \mathcal{T} informed by the pathogen genome sequences, latent continuous biological traits $\mathbf{x}_1, \dots, \mathbf{x}_n \in \mathbb{R}^m$ follows Brownian motion along the tree with an unknown $m \times m$ diffusion covariance $\boldsymbol{\Gamma}$ (Figure 6). The latent traits $\mathbf{x} = [\mathbf{x}_1, \dots, \mathbf{x}_n]$ map to the binary observation $\mathbf{y} \in \mathbb{R}^{m \times n}$ via the threshold model $y_{ij} = \mathbf{1}\{\mathbf{x}_{ij} > 0\} - \mathbf{1}\{\mathbf{x}_{ij} \leq 0\}$.

The model gives rise to a posterior distribution on the joint space $(\mathbf{x}, \boldsymbol{\Gamma}, \mathcal{T})$ of latent biological traits, diffusion covariance, and phylogenetic tree. To deal with this complex space, Zhang et al. (2019) deploys a Gibbs sampler, the computational bottleneck of which is updating \mathbf{x} from its full conditional — a $11,235 = 21 \times 535$ dimensional trun-

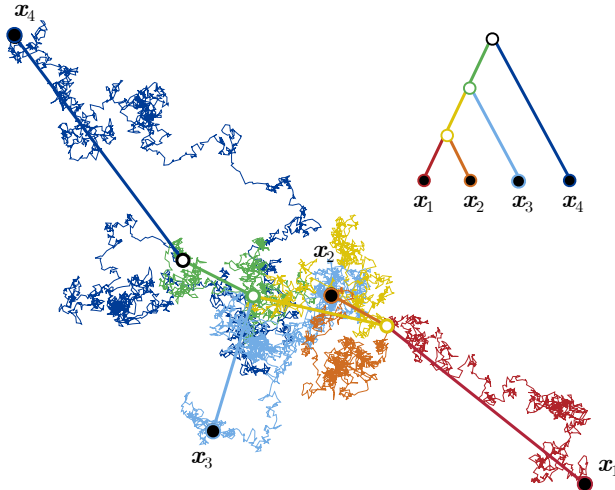


Fig. 6. Example path of latent biological traits following the phylogenetic Brownian diffusion. The traits of two distinct organisms evolve together until a branching event. Beyond that point, the traits evolve independently but with the same diffusion covariance induced by a shared bio-molecular mechanism.

Table 2. Relative ESS per computing time under the phylogenetic probit posterior ($d = 11,235$).

Phylogenetic probit	Relative ESS per time	
	min	PC
Markovian	1	1
Zigzag-NUTS	6.5	19

cated multivariate Gaussian. The $mn \times mn$ precision matrix $\Phi = \Phi(\Gamma, \mathcal{T})$ of $\mathbf{x} | \Gamma, \mathcal{T}$ induced by the phylogenetic Brownian diffusion model changes at each Gibbs iteration, precluding use of sampling algorithms that require expensive pre-processings of Φ . For the purpose of our simulation, we fix Γ at the highest posterior probability sample and \mathcal{T} at the maximum clade credibility tree obtained from the prior analysis by Zhang et al. (2019). Our target then is the distribution $\mathbf{x} | \Gamma, \mathcal{T} \sim \mathcal{N}(\boldsymbol{\mu}(\Gamma, \mathcal{T}), \Phi^{-1}(\Gamma, \mathcal{T}))$ truncated to $\{\text{sign}(\mathbf{x}) = \mathbf{y}\}$. There are 404 (3.6%) missing entries in \mathbf{y} and the target remains unconstrained along these coordinates. The target distribution parameters $\boldsymbol{\mu}$, Φ , and \mathbf{y} are publicly available on a Zenodo repository at <http://doi.org/10.5281/zenodo.4679720>.

On this real-world posterior, Hamiltonian zigzag again outperforms its Markovian counterpart — 6.5-fold increase in the minimum ESS across the coordinates and 19-fold increase in the ESS along the principal eigenvector of $\Phi^{-1}(\Gamma, \mathcal{T})$ (Table 2). There is no simple way to characterize the underlying correlation structure for this non-synthetic posterior, so we provide a histogram of the pairwise correlations in Figure 7 as a crude descriptive summary. We in particular find that only 0.00156% of correlations have magnitudes above 0.9. Apparently, however, the joint structure, truncation, and high-dimensionality together make for a complex target, which Hamiltonian zigzag can explore more efficiently by virtue of its full momentum.

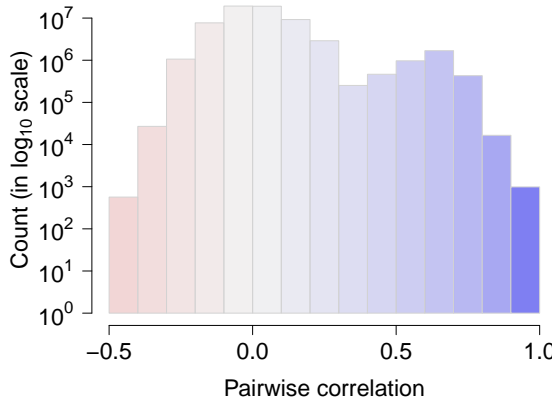


Fig. 7. Histogram of the pairwise correlations, i.e. the upper off-diagonal entries of $\Phi^{-1}(\Gamma, \mathcal{T})$, in the phylogenetic probit posterior. The vertical axis is in \log_{10} scale. No correlation falls outside the horizontal plot range $[-0.5, 1.0]$, with the smallest and largest correlation being -0.416 and 0.989 . Out of $mn(mn - 1)/2 \approx 63.1 \times 10^6$ correlations, 55.3×10^6 (87.6%) lie within $[-0.2, 0.2]$ and 987 (0.00156%) within $[0.9, 1]$.

5. Discussion

In recent years, both piecewise deterministic Markov process samplers (PDMP) and HMC have garnered intense research interests as potential game changers for Bayesian computation. In this article, we established that one of the most prominent PDMP is actually a close cousin of HMC, differing only in the amount of “momentum” they are born with. This revelation provided novel insights into relative performance of the two samplers, demonstrated via the practically relevant case of truncated multivariate Gaussian targets.

The uncovered relation between two zigzags begs the question: *is there a more general relationship between PDMP and HMC?* In particular, *can we add “momentum” to other versions of PDMP and improve their efficiency?* An affirmative answer to these questions, if possible, would necessarily require us to go beyond the current HMC framework based on classical Hamiltonian dynamics. The choice of deterministic dynamics underlying PDMP is in general not limited to Hamiltonian ones (Davis, 1993). Also, discontinuous changes in velocity seen in PDMP cannot be imitated by smooth Hamiltonian dynamics; such behavior was possible under Hamiltonian zigzag only because of its non-differentiable momentum distribution.

In a sense, our result shows that HMC’s momentum is really made of two components: direction and magnitude of inertia. PDMP’s velocity on the other hand consists only of direction. We suspect it is possible to introduce a notion of inertia magnitudes to PDMP in the form of auxiliary parameters — these parameters can interact with the main parameters so as to emulate the behavior of HMC, preserving the total log-density and storing inertia obtained from potential energy downhills for later use. Further investigation of this idea, however, is to be left for future research.

HMC is a relatively mature algorithm with a number of theoretical and algorithmic tools built around it over years of research. PDMP is a relative newcomer with exciting possibilities but also with many unanswered questions. Unification of the two frameworks could provide fertile grounds for further novel developments in Monte Carlo methods.

A. Proof of Lemma 3.2

The intuition behind our proof below of Lemma 3.2 is as follows. On the interval $[n\Delta t, (n+1)\Delta t]$, two or more velocity switch events occur only with the negligible probability of $O(\Delta t^2)$, allowing us to focus on the case of zero or one event. When starting from the same position and velocity, our coupling of $(\mathbf{x}_{\Delta t}^H, \mathbf{v}_{\Delta t}^H)$ and $(\mathbf{x}_{\Delta t}^M, \mathbf{v}_{\Delta t}^M)$ implies that, if Markovian zigzag does not experience any event on $[n\Delta t, (n+1)\Delta t]$, neither does Hamiltonian zigzag. Otherwise, when Markovian zigzag undergoes its first event, with high probability Hamiltonian zigzag experiences the same velocity switch at the exact same moment.

In bounding the probabilities of various events in the proof, we use the fact that zigzag velocities only take values in $\{\pm 1\}^d$ and hence, regardless of their actual trajectories, $\mathbf{x}_{\Delta t}^H(t)$ and $\mathbf{x}_{\Delta t}^M(t)$ stay within the L^∞ -ball $B_{\Delta t}$ around the initial position.

PROOF. We assume without loss of generality $n = 0$ as the proof is essentially identical for all n . Throughout the proof, all the discussed events are conditioned on $(\mathbf{x}_{\Delta t}^H, \mathbf{v}_{\Delta t}^H)(0) = (\mathbf{x}_{\Delta t}^M, \mathbf{v}_{\Delta t}^M)(0) = (\mathbf{x}_0, \mathbf{v}_0)$, but we do not explicitly denote the conditioning to avoid notational clutter. For $i = 1, \dots, d$, define indicator variables

$$I_i = \mathbb{1} \left\{ |p_{\Delta t, i}^H(0)| = -\log u_{0, i} \leq \int_0^{\Delta t} [v_{0, i} \partial_i U(\mathbf{x}_0 + s\mathbf{v}_0)]^+ ds \right\},$$

where $I_i = 1$ indicates the possibility of the velocity sign change along the i -th coordinate during the interval $[0, \Delta t]$. We partition the probability space into three types of events based on how many I_i 's equal 1:

$$\{I_i = 0 \text{ for all } i\} \text{ or } \bigcup_{i=1}^d \{I_i = 1, I_j = 0 \text{ for } j \neq i\} \text{ or } \bigcup_{1 \leq i < j \leq d} \{I_i = I_j = 1\}. \quad (22)$$

Below we analyze implications of each event type on the trajectory of $(\mathbf{x}_{\Delta t}^H, \mathbf{v}_{\Delta t}^H)$ and $(\mathbf{x}_{\Delta t}^M, \mathbf{v}_{\Delta t}^M)$ on $[0, \Delta t]$. We first establish that

$$\{I_i = 0 \text{ for all } i\} \subset \{(\mathbf{x}_{\Delta t}^H, \mathbf{v}_{\Delta t}^H) \equiv (\mathbf{x}_{\Delta t}^M, \mathbf{v}_{\Delta t}^M) \text{ on } [0, \Delta t]\}, \quad (23)$$

and that

$$\mathbb{P}\{I_i = I_j = 1\} \leq L_{\Delta t}(\mathbf{x}_0)^2 \Delta t^2 \text{ for } i < j. \quad (24)$$

We then show that, if $|\partial_i U(\mathbf{x}_0)| > \kappa_{\Delta t}(\mathbf{x}_0) \sqrt{d} \Delta t$,

$$\begin{aligned} \mathbb{P}(\{I_i = 1, I_j = 0 \text{ for } j \neq i\} \setminus \{(\mathbf{x}_{\Delta t}^H, \mathbf{v}_{\Delta t}^H) \equiv (\mathbf{x}_{\Delta t}^M, \mathbf{v}_{\Delta t}^M) \text{ on } [0, \Delta t]\}) \\ \leq 2L_{\Delta t}(\mathbf{x}_0)(d-1)\Delta t^2 \end{aligned} \quad (25)$$

and otherwise

$$\mathbb{P}\{I_i = 1, I_j = 0 \text{ for } j \neq i\} \leq 2\kappa_{\Delta t}(\mathbf{x}_0)\sqrt{d}\Delta t^2. \quad (26)$$

Once we establish the results (23) – (26), combined with the partition (22) of probability space, they imply that

$$\begin{aligned} 1 - \mathbb{P}\{(\mathbf{x}_{\Delta t}^H, \mathbf{v}_{\Delta t}^H) \equiv (\mathbf{x}_{\Delta t}^M, \mathbf{v}_{\Delta t}^M) \text{ on } [0, \Delta t]\} \\ \leq \frac{1}{2}L_{\Delta t}(\mathbf{x}_0)^2 d(d-1)\Delta t^2 + 2 \max\{\kappa_{\Delta t}(\mathbf{x}_0)d^{3/2}, L_{\Delta t}(\mathbf{x}_0)d^2\} \Delta t^2, \end{aligned}$$

completing the proof.

We first deal with the event type $\{I_i = 0 \text{ for all } i\}$. Note that

$$\{I_i = 0\} = \left\{ \int_0^{\Delta t} v_{0,i} \partial_i U(\mathbf{x}_0 + s\mathbf{v}_0) ds \leq \int_0^{\Delta t} [v_{0,i} \partial_i U(\mathbf{x}_0 + s\mathbf{v}_0)]^+ ds < -\log u_{0,i} \right\}.$$

In other words, $I_i = 0$ implies the lack of a velocity change along the i -th coordinate for both Hamiltonian and Markovian zigzag. If $I_i = 0$ for all i , therefore, the two zigzags thus stay along the line $\mathbf{x}(t) = \mathbf{x}_0 + t\mathbf{v}_0$ with the constant velocity $\mathbf{v}(t) = \mathbf{v}_0$ on $[0, \Delta t]$. This establishes (23).

To study implications of the event type $\{I_i = I_j = 1\}$ for $i < j$, note that

$$\int_0^{\Delta t} [v_{0,i} \partial_i U(\mathbf{x}_0 + s\mathbf{v}_0)]^+ ds \leq \max_{B_{\Delta t}(\mathbf{x}_0)} |\partial_i U| \Delta t.$$

It follows that

$$\begin{aligned} \mathbb{P}\{I_i = I_j = 1\} &\leq \mathbb{P}\left\{ -\log u_{0,i} \leq L_{\Delta t}(\mathbf{x}_0) \Delta t, -\log u_{0,j} \leq L_{\Delta t}(\mathbf{x}_0) \Delta t \right\} \\ &= [1 - \exp(-L_{\Delta t}(\mathbf{x}_0) \Delta t)]^2, \end{aligned}$$

from which (24) follows by observing that $\exp(-\epsilon) \geq 1 - \epsilon$ and hence $1 - \exp(-\epsilon) \leq \epsilon$.

We now turn to the event type $\{I_i = 1, I_j = 0 \text{ for } j \neq i\}$. In case $|\partial_i U(\mathbf{x}_0)| \leq \kappa_{\Delta t}(\mathbf{x}_0) \sqrt{d} \Delta t$, we have $|\partial_i U(\mathbf{x}_0 + s\mathbf{v}_0)| \leq 2\kappa_{\Delta t}(\mathbf{x}_0) \sqrt{d} \Delta t$ for $s \in [0, \Delta t]$ and obtain (26) by observing that

$$\begin{aligned} \mathbb{P}\{I_i = 1, I_j = 0 \text{ for } j \neq i\} &\leq \mathbb{P}\{I_i = 1\} \\ &= \mathbb{P}\left\{ -\log u_{0,i} \leq \int_0^{\Delta t} [v_{0,i} \partial_i U(\mathbf{x}_0 + s\mathbf{v}_0)]^+ ds \right\} \\ &\leq \mathbb{P}\left\{ -\log u_{0,i} \leq 2\kappa_{\Delta t}(\mathbf{x}_0) \sqrt{d} \Delta t^2 \right\} \\ &\leq 2\kappa_{\Delta t}(\mathbf{x}_0) \sqrt{d} \Delta t^2. \end{aligned}$$

Finally, we consider the case $|\partial_i U(\mathbf{x}_0)| > \kappa_{\Delta t}(\mathbf{x}_0) \sqrt{d} \Delta t$ under the event type $\{I_i = 1, I_j = 0 \text{ for } j \neq i\}$. We first focus on behavior of the two zigzags along the i -th coordinate since, within the event $\{I_j = 0 \text{ for } j \neq i\}$, the first velocity changes on $[0, \Delta t]$ can only occur in the i -th component. The condition $|\partial_i U(\mathbf{x}_0)| > \kappa_{\Delta t}(\mathbf{x}_0) \sqrt{d} \Delta t$ guarantees that the sign of $\partial_i U$ is constant on $B_{\Delta t}(\mathbf{x}_0)$ and along both zigzags' trajectories on $[0, \Delta t]$. In particular, we have either $v_{0,i} \partial_i U(\mathbf{x}_0 + s\mathbf{v}_0) < 0$ for all $s \in [0, \Delta t]$ or $v_{0,i} \partial_i U(\mathbf{x}_0 + s\mathbf{v}_0) > 0$ for all $s \in [0, \Delta t]$. The former would imply, combined with the condition $I_i = 1$, an impossibility $-\log u_{0,i} \leq \int_0^{\Delta t} [v_{0,i} \partial_i U(\mathbf{x}_0 + s\mathbf{v}_0)]^+ ds = 0$. Therefore, we must instead have $v_{0,i} \partial_i U(\mathbf{x}_0 + s\mathbf{v}_0) > 0$ for all $s \in [0, \Delta t]$. This implies that

$$\int_0^{\Delta t} v_{0,i} \partial_i U(\mathbf{x}_0 + s\mathbf{v}_0) ds = \int_0^{\Delta t} [v_{0,i} \partial_i U(\mathbf{x}_0 + s\mathbf{v}_0)]^+ ds$$

and that both zigzags undergo the first velocity change $v_{\Delta t,i}^H(\tau_0^{(1)}) = v_{\Delta t,i}^M(\tau_0^{(1)}) = -v_{0,i}$ at the same exact moment $\tau_0^{(1)}$. With this new velocity, we have $-v_{0,i} \partial_i U < 0$ on $B_{\Delta t}(\mathbf{x}_0)$ and hence there is no further change in $v_{\Delta t,i}^H(t)$ or $v_{\Delta t,i}^M(t)$ during $t \in [\tau_0^{(1)}, \tau_0^{(1)} + \Delta t]$.

We have so far shown that, under the assumed event type and condition on $|\partial_i U(\mathbf{x}_0)|$, 1) the two zigzags stay together on $[0, \Delta t]$ up to the first velocity change and 2) an additional velocity change, which could cause their paths to diverge, cannot occur along the i -th coordinate. In particular, the two zigzag paths on $[0, \Delta t]$ would diverge only if there were a sign change in the j -th velocity component for some $j \neq i$. We now show that such events occur with probability at most $O(\Delta t^2)$ within the event $\{I_j = 0 \text{ for } j \neq i\}$, thereby establishing (25).

We start by observing that the difference in integrals will be small on $[0, \Delta t]$ regardless of realized zigzag trajectories:

$$\int_0^{\Delta t} v_{\Delta t, j}^H(s) \partial_j U(\mathbf{x}_{\Delta t}^H(s)) ds \leq \int_0^{\Delta t} v_{0, j} \partial_j U(\mathbf{x}_0 + s\mathbf{v}_0) ds + 2L_{\Delta t}(\mathbf{x}_0)\Delta t^2 \quad (27)$$

as $|\partial_j U(\mathbf{x}) - \partial_j U(\mathbf{x}')| \leq 2L_{\Delta t}(\mathbf{x}_0)\Delta t$ for any $\mathbf{x}, \mathbf{x}' \in B_{\Delta t}(\mathbf{x}_0)$. Similarly,

$$\int_0^{\Delta t} [v_{\Delta t, j}^M(s) \partial_j U(\mathbf{x}_{\Delta t}^M(s))]^+ ds \leq \int_0^{\Delta t} [v_{0, j} \partial_j U(\mathbf{x}_0 + s\mathbf{v}_0)]^+ ds + 2L_{\Delta t}(\mathbf{x}_0)\Delta t^2. \quad (28)$$

We then observe that

$$\begin{aligned} & \{v_{\Delta t, j}^H \not\equiv v_{\Delta t, j}^M \text{ on } [0, \Delta t]\} \\ & \subset \left\{ \begin{array}{l} -\log u_{0, j} \leq \int_0^{\Delta t} v_{\Delta t, j}^H(s) \partial_j U(\mathbf{x}_{\Delta t}^H(s)) ds \\ \text{or} \quad -\log u_{0, j} \leq \int_0^{\Delta t} [v_{\Delta t, j}^M(s) \partial_j U(\mathbf{x}_{\Delta t}^M(s))]^+ ds \end{array} \right\} \\ & \subset \left\{ -\log u_{0, j} \leq \int_0^{\Delta t} [v_{0, j} \partial_j U(\mathbf{x}_0 + s\mathbf{v}_0)]^+ ds + 2L_{\Delta t}(\mathbf{x}_0)\Delta t^2 \right\}, \end{aligned} \quad (29)$$

where the latter inclusion follows from (27) and (28). The inclusion (29) implies that

$$\begin{aligned} & \mathbb{P}\{I_j = 0, v_{\Delta t, j}^H \not\equiv v_{\Delta t, j}^M \text{ on } [0, \Delta t]\} \\ & \leq \mathbb{P}\left\{ \begin{array}{l} \int_0^{\Delta t} [v_{0, j} \partial_j U(\mathbf{x}_0 + s\mathbf{v}_0)]^+ ds < -\log u_{0, j} \\ \leq \int_0^{\Delta t} [v_{0, j} \partial_j U(\mathbf{x}_0 + s\mathbf{v}_0)]^+ ds + 2L_{\Delta t}(\mathbf{x}_0)\Delta t^2 \end{array} \right\} \\ & \leq 2L_{\Delta t}(\mathbf{x}_0)\Delta t^2. \end{aligned}$$

We can now conclude (25) as follows:

$$\begin{aligned} & \mathbb{P}\{I_i = 1, I_j = 0 \text{ for all } j \neq i, (\mathbf{x}_{\Delta t}^H, \mathbf{v}_{\Delta t}^H) \not\equiv (\mathbf{x}_{\Delta t}^M, \mathbf{v}_{\Delta t}^M) \text{ on } [0, \Delta t]\} \\ & = \mathbb{P}\{I_i = 1, I_j = 0 \text{ for all } j \neq i, v_{\Delta t, j}^H \not\equiv v_{\Delta t, j}^M \text{ on } [0, \Delta t] \text{ for some } j \neq i\} \\ & \leq \mathbb{P}\{I_j = 0 \text{ for all } j \neq i, v_{\Delta t, j}^H \not\equiv v_{\Delta t, j}^M \text{ on } [0, \Delta t] \text{ for some } j \neq i\} \\ & \leq \sum_{j \neq i} \mathbb{P}\{I_j = 0, v_{\Delta t, j}^H \not\equiv v_{\Delta t, j}^M \text{ on } [0, \Delta t]\} \\ & \leq 2(d-1)L_{\Delta t}(\mathbf{x}_0)\Delta t^2. \end{aligned}$$

□

B. Efficient zigzags on truncated Gaussians

Here we describe how to simulate Hamiltonian and Markovian zigzag on a target distribution $\mathbf{x} \sim \mathcal{N}(\boldsymbol{\mu}, \boldsymbol{\Phi}^{-1})$ truncated to $\{\text{sign}(\mathbf{x}) = \mathbf{y} \in \{\pm 1\}^d\}$. On the support of the target, we have $\nabla U(\mathbf{x}) = \boldsymbol{\Phi}(\mathbf{x} - \boldsymbol{\mu})$ and hence

$$\begin{aligned} \int_0^t \nabla U(\mathbf{x} + s\mathbf{v}) \, ds &= \int_0^t (\boldsymbol{\varphi}_{\mathbf{x}} + s\boldsymbol{\varphi}_{\mathbf{v}}) \, ds \\ &= t\boldsymbol{\varphi}_{\mathbf{x}} + \frac{t^2}{2}\boldsymbol{\varphi}_{\mathbf{v}} \quad \text{where } \boldsymbol{\varphi}_{\mathbf{x}} = \boldsymbol{\Phi}(\mathbf{x} - \boldsymbol{\mu}) \text{ and } \boldsymbol{\varphi}_{\mathbf{v}} = \boldsymbol{\Phi}\mathbf{v}. \end{aligned} \quad (30)$$

In particular, the formula for the velocity switch event of Line 7 in Algorithm 1 becomes

$$t_i = \inf_{t>0} \left\{ |p_i| = v_i \int_0^t (\boldsymbol{\varphi}_{\mathbf{x},i} + s\boldsymbol{\varphi}_{\mathbf{v},i}) \, ds \right\} = \inf_{t>0} \left\{ p_i = t\boldsymbol{\varphi}_{\mathbf{x},i} + \frac{t^2}{2}\boldsymbol{\varphi}_{\mathbf{v},i} \right\}. \quad (31)$$

Determining t_i thus amounts to solving a quadratic equation with constraint.

We can handle the truncation via the technique of Neal (2010). Essentially, when the trajectory reaches a boundary $\{x_i = 0\}$, Hamiltonian zigzag bounces off against it, causing an instantaneous momentum and velocity flip $p_i \leftarrow -p_i$ and $v_i \leftarrow -v_i$. The trajectory then continues with these new momentum and velocity. In an algorithm implementation, this amounts to checking for velocity switch events caused by domain boundaries in addition to the native ones caused by the gradient ∇U guiding the dynamics.

Algorithm 3 provides pseudo code for simulating Hamiltonian zigzag on a multivariate Gaussian truncated to $\{\text{sign}(\mathbf{x}) = \mathbf{y} \in \{\pm 1\}^d\}$. Line 12 – 15 deal with the truncation, while the rest is essentially a target-specific version of Algorithm 1 with the analytical calculations (30) and (31) incorporated. The function `MINPOSITIVEROOT(a, b, c)`, vectorized in the pseudo code, returns the (smaller) positive root of the quadratic equation $at^2 + bt + c$ if it exists and ∞ otherwise. After updating \mathbf{x} and \mathbf{v} in Line 21 and 24, we can exploit the relations of Line 25 and 26 to avoid recomputing the matrix-vector products $\boldsymbol{\Phi}\mathbf{x}$ and $\boldsymbol{\Phi}\mathbf{v}$ from scratch. Note that, while the velocity update $\mathbf{v}_{\text{new}} = \mathbf{v}_{\text{old}} - 2v_{\text{old},i^*}\mathbf{e}_{i^*}$ corresponds to $\boldsymbol{\Phi}\mathbf{v}_{\text{new}} = \boldsymbol{\Phi}\mathbf{v}_{\text{old}} - 2v_{\text{old},i^*}\boldsymbol{\Phi}\mathbf{e}_{i^*}$, the sign in front of v_{i^*} in Line 26 appears flipped as the velocity has already been updated.

Algorithm 3 Hamiltonian zigzag on truncated Gaussian simulated for $t \in [0, T]$

```

1: function HAMILTONIANZIGZAG( $\mathbf{x}, \mathbf{p}, T$ )
2:    $\tau \leftarrow 0$ 
3:    $\mathbf{v} \leftarrow \text{sign}(\mathbf{p})$ 
4:    $\varphi_{\mathbf{x}} \leftarrow \Phi \mathbf{x}$ 
5:    $\varphi_{\mathbf{v}} \leftarrow \Phi \mathbf{v}$ 
6:   while  $\tau < T$  do
7:
8:
9:    $\mathbf{c} \leftarrow -\mathbf{p}$ 
10:   $\mathbf{t}_{\text{grad}} \leftarrow$ 
     MINPOSITIVEROOT( $\frac{1}{2}\varphi_{\mathbf{v}}, \varphi_{\mathbf{x}}, \mathbf{c}$ )
11:   $t_{\text{grad}}^* \leftarrow \min_i t_{\text{grad},i}$ 
12:   $\mathbf{t}_{\text{bdry}} = -\mathbf{x}/\mathbf{v}$ 
13:   $\mathbf{t}_{\text{bdry}}[\mathbf{t}_{\text{bdry}} < 0] \leftarrow \infty$ 
14:   $t_{\text{bdry}}^* \leftarrow \min_i t_{\text{bdry},i}$ 
15:   $t^* \leftarrow \min\{t_{\text{grad}}^*, t_{\text{bdry}}^*\}$ 
16:  if  $\tau + t^* > T$  then
17:     $\mathbf{x} \leftarrow \mathbf{x} + (T - \tau)\mathbf{v}$ 
18:     $\mathbf{p} \leftarrow \mathbf{p} - (T - \tau)\varphi_{\mathbf{x}} - (T - \tau)^2\varphi_{\mathbf{v}}/2$ 
19:     $\tau \leftarrow T$ 
20:  else
21:     $\mathbf{x} \leftarrow \mathbf{x} + t^*\mathbf{v}$ 
22:     $\mathbf{p} \leftarrow \mathbf{p} - t^*\varphi_{\mathbf{x}} - t^{*2}\varphi_{\mathbf{v}}/2$ 
23:     $i^* \leftarrow \text{argmin}_i t_i$ 
24:     $v_{i^*} \leftarrow -v_{i^*}$ 
25:     $\varphi_{\mathbf{x}} \leftarrow \varphi_{\mathbf{x}} + t^*\varphi_{\mathbf{v}}$ 
26:     $\varphi_{\mathbf{v}} \leftarrow \varphi_{\mathbf{v}} + 2v_{i^*}\Phi \mathbf{e}_{i^*}$ 
27:     $\tau \leftarrow \tau + t^*$ 
28:  end if
29: end while
30: return  $(\mathbf{x}, \mathbf{p})$ 
31: end function

```

Algorithm 4 Markovian zigzag on truncated Gaussian simulated for $t \in [0, T]$

```

1: function MARKOVIANZIGZAG( $\mathbf{x}, \mathbf{v}, T$ )
2:    $\tau \leftarrow 0$ 
3:
4:    $\varphi_{\mathbf{x}} \leftarrow \Phi \mathbf{x}$ 
5:    $\varphi_{\mathbf{v}} \leftarrow \Phi \mathbf{v}$ 
6:   while  $\tau < T$  do
7:      $\mathbf{u} \stackrel{\text{i.i.d.}}{\sim} \text{Unif}(0, 1)$ 
8:      $t^\dagger \leftarrow \text{FIRSTPOSITIVETIME}(\varphi_{\mathbf{v}}, \varphi_{\mathbf{x}})$ 
9:      $\mathbf{c} \leftarrow \log \mathbf{u} + t^\dagger \mathbf{v} \varphi_{\mathbf{v}} + \frac{1}{2} t^{\dagger 2} \mathbf{v} \varphi_{\mathbf{x}}$ 
10:     $\mathbf{t}_{\text{grad}} \leftarrow$ 
     MINPOSITIVEROOT $\geq t^\dagger$ ( $\frac{1}{2}\varphi_{\mathbf{v}}, \varphi_{\mathbf{x}}, \mathbf{c}$ )
11:     $t_{\text{grad}}^* \leftarrow \min_i t_{\text{grad},i}$ 
12:     $\mathbf{t}_{\text{bdry}} = -\mathbf{x}/\mathbf{v}$ 
13:     $\mathbf{t}_{\text{bdry}}[\mathbf{t}_{\text{bdry}} < 0] \leftarrow \infty$ 
14:     $t_{\text{bdry}}^* \leftarrow \min_i t_{\text{bdry},i}$ 
15:     $t^* \leftarrow \min\{t_{\text{grad}}^*, t_{\text{bdry}}^*\}$ 
16:    if  $\tau + t^* > T$  then
17:       $\mathbf{x} \leftarrow \mathbf{x} + (T - \tau)\mathbf{v}$ 
18:
19:       $\tau \leftarrow T$ 
20:    else
21:       $\mathbf{x} \leftarrow \mathbf{x} + t^*\mathbf{v}$ 
22:
23:       $i^* \leftarrow \text{argmin}_i t_i$ 
24:       $v_{i^*} \leftarrow -v_{i^*}$ 
25:       $\varphi_{\mathbf{x}} \leftarrow \varphi_{\mathbf{x}} + t^*\varphi_{\mathbf{v}}$ 
26:       $\varphi_{\mathbf{v}} \leftarrow \varphi_{\mathbf{v}} + 2v_{i^*}\Phi \mathbf{e}_{i^*}$ 
27:       $\tau \leftarrow \tau + t^*$ 
28:    end if
29: end while
30: return  $(\mathbf{x}, \mathbf{v})$ 
31: end function

```

For Markovian zigzag, we can take advantage of the following analytical expressions. Observe that

$$\begin{aligned}
\int_0^t [v_i \partial_i U(\mathbf{x} + s\mathbf{v})]^+ ds &= \int_{t_i^\dagger}^t (v_i \varphi_{\mathbf{x},i} + s v_i \varphi_{\mathbf{v},i}) ds \\
&= t v_i \varphi_{\mathbf{x},i} + \frac{t^2}{2} v_i \varphi_{\mathbf{v},i} - t_i^\dagger v_i \varphi_{\mathbf{x},i} - \frac{t_i^{\dagger 2}}{2} v_i \varphi_{\mathbf{v},i}
\end{aligned} \tag{32}$$

provided $t \geq t_i^\dagger$, where t_i^\dagger denotes the time, if it exists, at which the linear function $s \rightarrow v_i \varphi_{\mathbf{x},i} + s v_i \varphi_{\mathbf{x},i}$ on $s \geq 0$ attains a positive value for the first time. More precisely,

we define

$$t_i^\dagger := \begin{cases} -\varphi_{\mathbf{v},i}/\varphi_{\mathbf{x},i} & \text{if } v_i \varphi_{\mathbf{x},i} < 0 \text{ and } v_i \varphi_{\mathbf{v},i} \geq 0, \\ \infty & \text{if } v_i \varphi_{\mathbf{x},i} < 0 \text{ and } v_i \varphi_{\mathbf{v},i} < 0, \\ 0 & \text{otherwise.} \end{cases} \quad (33)$$

Using (32), we can express the velocity switch event formula of Line 7 in Algorithm 2 as

$$t_i = \inf_{t > t_i^\dagger} \left\{ -\log u_i = t v_i \varphi_{\mathbf{x},i} + \frac{t^2}{2} v_i \varphi_{\mathbf{v},i} - t_i^\dagger v_i \varphi_{\mathbf{x},i} - \frac{t_i^{\dagger 2}}{2} v_i \varphi_{\mathbf{v},i} \right\},$$

if the infimum exists and $t_i = \infty$ otherwise.

Algorithm 4 provides pseudo code for simulating Markovian zigzag on a multivariate Gaussian truncated to $\{\text{sign}(\mathbf{x}) = \mathbf{y} \in \{\pm 1\}^d\}$. The `FIRSTPOSITIVETIME`($\varphi_{\mathbf{v}}, \varphi_{\mathbf{x}}$) function computes t_i^\dagger 's as in (33). The expressions $\mathbf{t}^\dagger \mathbf{v} \varphi_{\mathbf{v}}$ and $\mathbf{t}^{\dagger 2} \mathbf{v} \varphi_{\mathbf{x}}$ in Line 9 denote element-wise multiplied vectors. The `MINPOSITIVEROOT` $_{\geq t_i^\dagger}(a, b, c)$ function returns the (smaller) positive root as in in Algorithm 3 but also requires the root to be greater than t_i^\dagger . The input c_i can be infinity here, in which case we require the function to return ∞ .

References

Andrieu, C. and Livingstone, S. (2019) Peskun-tierney ordering for markov chain and process Monte Carlo: beyond the reversible scenario. *arXiv:1906.06197*.

Bierkens, J. and Duncan, A. (2017) Limit theorems for the zig-zag process. *Advances in Applied Probability*, **49**, 791–825.

Bierkens, J., Fearnhead, P., Roberts, G. et al. (2019a) The zig-zag process and super-efficient sampling for Bayesian analysis of big data. *The Annals of Statistics*, **47**, 1288–1320.

Bierkens, J., Kamatani, K. and Roberts, G. O. (2018) High-dimensional scaling limits of piecewise deterministic sampling algorithms. *arXiv:1807.11358*.

Bierkens, J., Roberts, G. O., Zitt, P.-A. et al. (2019b) Ergodicity of the zigzag process. *The Annals of Applied Probability*, **29**, 2266–2301.

Billingsley, P. (1999) *Convergence of Probability Measures*. Wiley Series in Probability and Statistics. John Wiley & Sons Inc.

Botev, Z. I. (2017) The normal law under linear restrictions: simulation and estimation via minimax tilting. *Journal of the Royal Statistical Society: Series B (Statistical Methodology)*, **79**, 125–148.

Bou-Rabee, N. and Sanz-Serna, J. (2018) Geometric integrators and the Hamiltonian Monte Carlo method. *Acta Numerica*, **27**, 113–206.

Bouchard-Côté, A., Vollmer, S. J. and Doucet, A. (2018) The bouncy particle sampler: a non-reversible rejection-free Markov chain Monte Carlo method. *Journal of the American Statistical Association*, 1–13.

Carpenter, B., Gelman, A., Hoffman, M. D., Lee, D., Goodrich, B., Betancourt, M., Brubaker, M., Guo, J., Li, P. and Riddell, A. (2017) Stan: A probabilistic programming language. *Journal of Statistical Software*, **76**.

Davis, M. H. (1993) *Markov models & optimization*. CRC Press.

De Gosson, M. A. (2011) *Symplectic methods in harmonic analysis and in mathematical physics*, vol. 7. Springer.

Duane, S., Kennedy, A. D., Pendleton, B. J. and Roweth, D. (1987) Hybrid Monte Carlo. *Physics letters B*, **195**, 216–222.

Dunson, D. B. and Johndrow, J. (2020) The Hastings algorithm at fifty. *Biometrika*, **107**, 1–23.

Ethier, S. N. and Kurtz, T. G. (2005) *Markov processes: characterization and convergence*. John Wiley & Sons.

Fang, Y., Sanz-Serna, J.-M. and Skeel, R. D. (2014) Compressible generalized hybrid Monte Carlo. *The Journal of chemical physics*, **140**, 174108.

Fearnhead, P., Bierkens, J., Pollock, M., Roberts, G. O. et al. (2018) Piecewise deterministic Markov processes for continuous-time Monte Carlo. *Statistical Science*, **33**, 386–412.

Fetecau, R. C., Marsden, J. E., Ortiz, M. and West, M. (2003) Nonsmooth Lagrangian mechanics and variational collision integrators. *SIAM Journal on Applied Dynamical Systems*, **2**, 381–416.

Filippov, A. F. (1988) *Differential equations with discontinuous righthand sides*. Kluwer Academic Publishers.

Geyer, C. (2011) Introduction to Markov chain Monte Carlo. In *Handbook of Markov Chain Monte Carlo*, 3–48. CRC Press.

Guntheroth, K. (2016) *Optimized C++: Proven Techniques for Heightened Performance*. O'Reilly Media, Inc.

Hoffman, M. D. and Gelman, A. (2014) The no-U-turn sampler: adaptively setting path lengths in Hamiltonian Monte Carlo. *Journal of Machine Learning Research*, **15**, 1593–1623.

Holbrook, A. J., Lemey, P., Baele, G., Dellicour, S., Brockmann, D., Rambaut, A. and Suchard, M. A. (2020) Massive parallelization boosts big bayesian multidimensional scaling. *Journal of Computational and Graphical Statistics*, 1–34.

Khulief, Y. (2013) Modeling of impact in multibody systems: an overview. *Journal of Computational and Nonlinear Dynamics*, **8**.

Meurant, G. A. (2006) *The Lanczos and Conjugate Gradient Algorithms: from Theory to Finite Precision Computations*. Society for Industrial and Applied Mathematics.

Neal, R. M. (1996) *Bayesian Learning for Neural Networks*. Springer-Verlag.

— (2010) MCMC using Hamiltonian Dynamics. In *Handbook of Markov chain Monte Carlo*. CRC Press.

— (2012) No U-turns for Hamiltonian Monte Carlo — comments on a paper by Hoffman and Gelman. <https://radfordneal.wordpress.com/2012/01/21/no-u-turns-for-hamiltonian-monte-carlo-comments-on-a-paper-by-hoffman-and-gelman/>.

Nishimura, A. and Dunson, D. (2020) Recycling intermediate steps to improve Hamiltonian Monte Carlo. *Bayesian Analysis*, **15**, 1087–1108.

Nishimura, A., Dunson, D. and Lu, J. (2020) Discontinuous Hamiltonian Monte Carlo for discrete parameters and discontinuous likelihoods. *Biometrika*.

Nishimura, A. and Suchard, M. A. (2018) Supplement to “prior-preconditioned conjugate gradient for accelerated gibbs sampling in ‘large n & large p’ sparse bayesian logistic regression models”. *arXiv:1810.12437*.

Pakman, A. and Paninski, L. (2014) Exact Hamiltonian Monte Carlo for truncated multivariate gaussians. *Journal of Computational and Graphical Statistics*, **23**, 518–542.

Peters, E. A. J. F. and de With, G. (2012) Rejection-free Monte Carlo sampling for general potentials. *Physical Review E*, **85**, 026703.

Plummer, M., Best, N., Cowles, K. and Vines, K. (2006) CODA: Convergence diagnosis and output analysis for MCMC. *R News*, **6**, 7–11.

Salvatier, J., Wiecki, T. V. and Fonnesbeck, C. (2016) Probabilistic programming in Python using PyMC3. *PeerJ Computer Science*, **2**, e55.

Spivak, M. (1965) *Calculus on manifolds: a modern approach to classical theorems of advanced calculus*. Addison-Wesley.

Suchard, M. A., Lemey, P., Baele, G., Ayres, D. L., Drummond, A. J. and Rambaut, A. (2018) Bayesian phylogenetic and phylodynamic data integration using BEAST 1.10. *Virus evolution*, **4**, vey016.

Turitsyn, K. S., Chertkov, M. and Vucelja, M. (2011) Irreversible Monte Carlo algorithms for efficient sampling. *Physica D: Nonlinear Phenomena*, **240**, 410–414.

Vanetti, P., Bouchard-Côté, A., Deligiannidis, G. and Doucet, A. (2017) Piecewise-deterministic Markov chain Monte Carlo. *arXiv:1707.05296*.

Wang, Z., Mohamed, S. and Freitas, N. (2013) Adaptive Hamiltonian and Riemann manifold Monte Carlo. In *Proceedings of the 30th International Conference on Machine Learning*, 1462–1470.

Wu, C., Stoehr, J. and Robert, C. P. (2018) Faster Hamiltonian Monte Carlo by learning leapfrog scale. *arXiv:1810.04449*.

Zhang, Z., Nishimura, A., Bastide, P., Ji, X., Payne, R. P., Goulder, P., Lemey, P. and Suchard, M. A. (2019) Large-scale inference of correlation among mixed-type biological traits with Phylogenetic multivariate probit models. *arXiv:1912.09185*.

Supplement to “Hamiltonian zigzag sampler got more momentum than its Markovian counterpart: Equivalence of two zigzags under a momentum refreshment limit”

S1. Proof of Theorem 2.1

In the proofs below, we use the following standard terminologies. A *solution operator* $\{\Psi_t\}_{t \geq 0}$ of a differential equation is a family of maps such that Ψ_0 acts as the identity and $(\mathbf{x}_t, \mathbf{p}_t) = \Psi_t(\mathbf{x}, \mathbf{p})$ for $t \geq 0$ constitutes a solution of the given equation. The dynamics associated with a differential equation is *time-reversible* if $\mathbf{R} \circ \Psi_t = (\mathbf{R} \circ \Psi_t)^{-1}$ where \mathbf{R} is the momentum flip operator $\mathbf{R}(\mathbf{x}, \mathbf{p}) = (\mathbf{x}, -\mathbf{p})$. In other words, the forward dynamic followed by the momentum flip can be undone by the exact same operation. Also, the dynamics is *symplectic* if

$$\frac{\partial(\mathbf{x}_t, \mathbf{p}_t)^\top}{\partial(\mathbf{x}, \mathbf{p})} \begin{bmatrix} \mathbf{0} & \mathbf{I} \\ -\mathbf{I} & \mathbf{0} \end{bmatrix} \frac{\partial(\mathbf{x}_t, \mathbf{p}_t)}{\partial(\mathbf{x}, \mathbf{p})} = \begin{bmatrix} \mathbf{0} & \mathbf{I} \\ -\mathbf{I} & \mathbf{0} \end{bmatrix} \quad (\text{S1})$$

for all $t \geq 0$, where \mathbf{I} denote the $d \times d$ identity matrix. The relation (S1) can be equivalently expressed as (De Gosson, 2011):

$$\frac{\partial \mathbf{x}_t}{\partial \mathbf{x}}^\top \frac{\partial \mathbf{p}_t}{\partial \mathbf{x}}, \frac{\partial \mathbf{x}_t}{\partial \mathbf{p}}^\top \frac{\partial \mathbf{p}_t}{\partial \mathbf{p}} \text{ are symmetric; } \frac{\partial \mathbf{x}_t}{\partial \mathbf{x}}^\top \frac{\partial \mathbf{p}_t}{\partial \mathbf{p}} - \frac{\partial \mathbf{p}_t}{\partial \mathbf{x}}^\top \frac{\partial \mathbf{x}_t}{\partial \mathbf{p}} = \mathbf{I}. \quad (\text{S2})$$

PROOF (OF EXISTENCE AND UNIQUENESS). As explained in Section 2.1, the solution is completely characterized by (3) – (8) as long as the trajectory stays away from the problematic set $S = \bigcup_i S_i$ for S_i as in (9). The conclusions therefore follow once we show the existence of the measure zero set Ω , starting away from which the trajectory described in Section 2.1 avoids S for all $t \geq 0$.

We construct Ω as a union of lower dimensional manifolds by backtracking states that may end up in S under the dynamics of (2). For brevity, we omit the adverb “at most” when referring to manifold dimensions and take the dimension of $\{\partial_i U(\mathbf{x}) = 0\}$ to be exactly $d - 1$, but the arguments equally hold when some of the manifolds are of lower dimensions. We first observe that, being a transversal intersection of two $(d - 1)$ -dimensional manifolds $\{(\mathbf{x}, \mathbf{p}) : \partial_i U(\mathbf{x}) = 0\}$ and $\{(\mathbf{x}, \mathbf{p}) : p_i = 0\}$, the set S_i is a $(d - 2)$ -dimensional manifold. We then consider a dynamics similar to (2) but with a fixed velocity $\mathbf{v} \in \{\pm 1\}^d$:

$$\frac{d\mathbf{x}}{dt} = \mathbf{v}, \quad \frac{d\mathbf{p}}{dt} = -\nabla U(\mathbf{x}). \quad (\text{S3})$$

Let $\Psi_{\mathbf{v}, -t}$ for $t \geq 0$ denote the solution operator of (S3) backward in time i.e.

$$\Psi_{\mathbf{v}, -t}(\mathbf{x}, \mathbf{p}) = \left(\mathbf{x} - t\mathbf{v}, \mathbf{p} + \int_0^t \nabla U(\mathbf{x} - s\mathbf{v}) ds \right).$$

By our construction, the set $\Omega^{(1)} = \bigcup_{i, \mathbf{v} \in \{\pm 1\}^d} \Omega_{i, \mathbf{v}}^{(1)}$ for

$$\Omega_{i, \mathbf{v}}^{(1)} = \bigcup_{t \geq 0} \Psi_{\mathbf{v}, -t}(S_i) \quad (\text{S4})$$

contains all the initial states from which the dynamics of (2) reaches S at the first velocity switch event. In other words, for all initial conditions $(\mathbf{x}(0), \mathbf{p}(0)) \notin \Omega^{(1)}$, the dynamics of (2) circumvents the problematic set S at least until the second velocity switch event. Moreover, each $\Omega_{i,\mathbf{v}}^{(1)}$ has measure zero because it is an image of the $(d-1)$ -dimensional manifold $[0, \infty) \times S_i$ under the continuously differentiable map $(t, \mathbf{x}, \mathbf{p}) \rightarrow \Psi_{\mathbf{v},-t}(\mathbf{x}, \mathbf{p})$.

We now address the question of whether the dynamics continues to avoid the problematic sets after the first event. Even if a trajectory starts away from the set $\Omega^{(1)}$, it could happen that $(\mathbf{x}(\tau), \mathbf{p}(\tau)) \in \Omega_{i,\mathbf{v}}^{(1)}$ at some time point τ , in which case the trajectory could encounter S_i at the next velocity switch event. Such a trajectory, having started outside $\Omega_{i,\mathbf{v}}^{(1)}$, can only enter $\Omega_{i,\mathbf{v}}^{(1)}$ at the moment of velocity switch and hence necessarily passes through the set

$$\bigcup_j \left[\Omega_{i,\mathbf{v}}^{(1)} \cap \{(\mathbf{x}, \mathbf{p}) : p_j = 0\} \right].$$

Consequently, the set $\Omega^{(2)} = \bigcup_{i,\mathbf{w} \in \{\pm 1\}^d} \Omega_{i,\mathbf{w}}^{(2)}$ for

$$\Omega_{i,\mathbf{w}}^{(2)} = \bigcup_{t \geq 0} \Psi_{\mathbf{w},-t} \left(\bigcup_{j,\mathbf{v}} \left[\Omega_{i,\mathbf{v}}^{(1)} \cap \{(\mathbf{x}, \mathbf{p}) : p_j = 0\} \right] \right)$$

contains all the initial states from which the dynamics of (2) reaches S at the second velocity switch event. We will now show that each $\Omega_{i,\mathbf{v}}^{(1)} \cap \{(\mathbf{x}, \mathbf{p}) : p_j = 0\}$ is contained in a $(d-2)$ -dimensional manifold. Following the same reasoning as for $\Omega_{i,\mathbf{v}}^{(1)}$, we can then conclude that each $\Omega_{i,\mathbf{w}}^{(2)}$ has measure zero.

To this end, as we already know S_j is a $(d-2)$ -dimensional manifold, it suffices to show that the intersection of $\Omega_{i,\mathbf{v}}^{(1)} \cap \{p_j = 0\}$ with S_j^c belongs to a $(d-2)$ -dimensional manifold. This follows from the fact that the two manifolds $\Omega_{i,\mathbf{v}}^{(1)}$ and $\{p_j = 0\}$ intersect transversally away from S_j . To show this, we study the tangent spaces at $(\mathbf{x}, \mathbf{p}) \in \Omega_{i,\mathbf{v}}^{(1)} \cap \{p_j = 0\} \cap S_j^c$. The tangent space of $\{p_j = 0\}$ spans all but the direction of the standard basis \mathbf{e}_{d+j} . On the other hand, by our construction (S4), the tangent space of $\Omega_{i,\mathbf{v}}^{(1)}$ at (\mathbf{x}, \mathbf{p}) includes the time derivative $\partial_t \Psi_{\mathbf{v},-t}(\mathbf{x}, \mathbf{p})$ evaluated at $t = 0$, whose $(d+j)$ -th component is given by

$$[\partial_t \Psi_{\mathbf{v},-0}(\mathbf{x}, \mathbf{p})]_{d+j} = [(-\mathbf{v}, \nabla U(\mathbf{x}))]_{d+j} = \partial_j U(\mathbf{x}) \neq 0,$$

where the last inequality holds because $(\mathbf{x}, \mathbf{p}) \notin S_j$. This proves that $\Omega_{i,\mathbf{v}}^{(1)} \cap \{p_j = 0\}$ is contained in a $(d-2)$ -dimensional manifold and hence that each $\Omega_{i,\mathbf{w}}^{(2)}$ has measure zero.

We have thus far shown that, when starting from the initial states outside the sets of measure zero $\Omega^{(1)}$ and $\Omega^{(2)}$, the dynamics of (2) avoids the problematic set S at least until the second velocity switch event. We can continue the construction in the same manner and, for $k \geq 2$, quantify a set $\Omega^{(k+1)}$ of measure zero that include all the initial states from which the dynamics may encounter S at the $(k+1)$ -th velocity switch event. We obtain the set in the theorem statement by taking the union $\Omega = \bigcup_i \Omega^{(i)}$. \square

PROOF (OF TIME-REVERSIBILITY AND SYMPLECTICITY). Since compositions of time-reversible and symplectic maps are again time-reversible and symplectic, by dividing up

the interval $[0, t]$ into smaller pieces if necessary, we can without loss of generality assume that there is at most one velocity switch event in the interval $[0, t]$.

For time-reversibility, we need to show that Hamiltonian zigzag satisfies, in the language of Algorithm 1,

$$(\mathbf{x}, -\mathbf{p}) = \text{HAMILTONIANZIGZAG}(\mathbf{x}^*, -\mathbf{p}^*, t) \\ \text{where } (\mathbf{x}^*, \mathbf{p}^*) = \text{HAMILTONIANZIGZAG}(\mathbf{x}, \mathbf{p}, t).$$

Verifying this is straightforward, so we focus on proving symplecticity.

We establish the symplecticity by directly calculating the derivatives of the solution $(\mathbf{x}_t, \mathbf{p}_t)$ with respect to the initial condition $(\mathbf{x}, \mathbf{p}) \notin \Omega$. In case there is no velocity switch event, we have

$$\mathbf{x}_t = \mathbf{x} + t\mathbf{v}, \quad \mathbf{p}_t = \mathbf{p} + \int_0^t \nabla U(\mathbf{x} + s\mathbf{v}) \, ds.$$

Differentiating $(\mathbf{x}_t, \mathbf{p}_t)$ with respect to (\mathbf{x}, \mathbf{p}) , we obtain

$$\frac{\partial \mathbf{x}_t}{\partial \mathbf{x}} = \mathbf{I}, \quad \frac{\partial \mathbf{x}_t}{\partial \mathbf{p}} = \mathbf{0}, \quad \frac{\partial \mathbf{p}_t}{\partial \mathbf{x}} = \int_0^t \nabla^2 U(\mathbf{x} + s\mathbf{v}) \, ds, \quad \frac{\partial \mathbf{p}_t}{\partial \mathbf{p}} = \mathbf{I}, \quad (\text{S5})$$

where $\nabla^2 U$ denotes the symmetric Hessian matrix. The symplecticity condition (S2) is easily verified from (S5).

We now deal with the case in which there is one velocity switch event on $[0, t]$. In this case, we have

$$\mathbf{x}_t = \mathbf{x} + t^* \mathbf{v} + (t - t^*) \mathbf{v}^* \quad \text{for } \mathbf{v} = \text{sign}(\mathbf{p}), \\ \mathbf{p}_t = \mathbf{p} + \int_0^{t^*} \nabla U(\mathbf{x} + s\mathbf{v}) \, ds + \int_{t^*}^t \nabla U(\mathbf{x} + t^* \mathbf{v} + (s - t^*) \mathbf{v}^*) \, ds, \quad (\text{S6})$$

where t^* and \mathbf{v}^* satisfy the following relations for some index i :

$$|p_i| = \int_0^{t^*} v_i \partial_i U(\mathbf{x} + s\mathbf{v}) \, ds, \\ v_i^* = -v_i \quad \text{and} \quad v_j^* = v_j \text{ for all } j \neq i.$$

To simplify the calculations to follow, we re-express (S6) as

$$\mathbf{x}_s = \mathbf{x} + s\mathbf{v}^* + 2t^* v_i \mathbf{e}_i \quad \text{for } s \in (t^*, t], \\ \mathbf{p}_t = \mathbf{p} + \int_0^{t^*} \nabla U(\mathbf{x} + s\mathbf{v}) \, ds + \int_{t^*}^t \nabla U(\mathbf{x}_s) \, ds. \quad (\text{S7})$$

We differentiate (S7) using Lemma S1.1 below and the chain rule. This yields

$$\frac{\partial \mathbf{x}_t}{\partial \mathbf{x}} = \frac{\partial \mathbf{x}_s}{\partial \mathbf{x}} = \mathbf{I} + 2v_i \mathbf{e}_i \frac{\partial t^*}{\partial \mathbf{x}} \quad \text{for } s \in [t^*, t], \quad (\text{S8})$$

$$\frac{\partial \mathbf{x}_t}{\partial \mathbf{p}} = 2v_i \mathbf{e}_i \frac{\partial t^*}{\partial \mathbf{p}} = \frac{2v_i}{\partial_i U(\mathbf{x}^*)} \mathbf{e}_i \mathbf{e}_i^\top, \quad (\text{S9})$$

$$\begin{aligned} \frac{\partial \mathbf{p}_t}{\partial \mathbf{x}} &= \nabla U(\mathbf{x}^*) \frac{\partial t^*}{\partial \mathbf{x}} - \nabla U(\mathbf{x}^*) \frac{\partial t^*}{\partial \mathbf{p}} + \int_0^{t^*} \nabla^2 U(\mathbf{x} + s\mathbf{v}) \, ds + \int_{t^*}^t \nabla^2 U(\mathbf{x}_s) \frac{\partial \mathbf{x}_s}{\partial \mathbf{x}} \, ds \\ &= \int_0^{t^*} \nabla^2 U(\mathbf{x} + s\mathbf{v}) \, ds + \left(\int_{t^*}^t \nabla^2 U(\mathbf{x}_s) \, ds \right) \frac{\partial \mathbf{x}_t}{\partial \mathbf{x}}, \end{aligned} \quad (\text{S10})$$

$$\begin{aligned} \frac{\partial \mathbf{p}_t}{\partial \mathbf{p}} &= \mathbf{I} + \nabla U(\mathbf{x}^*) \frac{\partial t^*}{\partial \mathbf{p}} - \nabla U(\mathbf{x}^*) \frac{\partial t^*}{\partial \mathbf{p}} + \int_{t^*}^t \nabla^2 U(\mathbf{x}_s) \frac{\partial \mathbf{x}_s}{\partial \mathbf{p}} \, ds \\ &= \mathbf{I} + \frac{2v_i}{\partial_i U(\mathbf{x}^*)} \left(\int_{t^*}^t \nabla^2 U(\mathbf{x}_s) \, ds \right) \mathbf{e}_i \mathbf{e}_i^\top. \end{aligned} \quad (\text{S11})$$

We now check the three conditions (S2) for symplecticity using the relations (S8) – (S11) and (S14). The symmetry of $(\partial \mathbf{x}_t / \partial \mathbf{p})^\top (\partial \mathbf{p}_t / \partial \mathbf{p})$ is trivial. The symmetry of $(\partial \mathbf{x}_t / \partial \mathbf{x})^\top (\partial \mathbf{p}_t / \partial \mathbf{x})$ follows by noting that

$$\begin{aligned} \frac{\partial \mathbf{x}_t}{\partial \mathbf{x}}^\top \frac{\partial \mathbf{p}_t}{\partial \mathbf{x}} &= \frac{\partial \mathbf{x}_t}{\partial \mathbf{x}}^\top \left(\int_0^{t^*} \nabla^2 U(\mathbf{x} + s\mathbf{v}) \, ds \right) + \frac{\partial \mathbf{x}_t}{\partial \mathbf{x}}^\top \left(\int_{t^*}^t \nabla^2 U(\mathbf{x}_s) \, ds \right) \frac{\partial \mathbf{x}_t}{\partial \mathbf{x}} \\ &= \int_0^{t^*} \nabla^2 U(\mathbf{x} + s\mathbf{v}) \, ds + 2v_i \partial_i U(\mathbf{x}^*) \frac{\partial t^*}{\partial \mathbf{x}}^\top \frac{\partial t^*}{\partial \mathbf{x}} + \frac{\partial \mathbf{x}_t}{\partial \mathbf{x}}^\top \left(\int_{t^*}^t \nabla^2 U(\mathbf{x}_s) \, ds \right) \frac{\partial \mathbf{x}_t}{\partial \mathbf{x}}, \end{aligned}$$

where each term is clearly symmetric in the last expression. Finally, we observe that

$$\begin{aligned} \frac{\partial \mathbf{x}_t}{\partial \mathbf{x}}^\top \frac{\partial \mathbf{p}_t}{\partial \mathbf{p}} &= \frac{\partial \mathbf{x}_t}{\partial \mathbf{x}}^\top \left[\mathbf{I} + \frac{2v_i}{\partial_i U(\mathbf{x}^*)} \left(\int_{t^*}^t \nabla^2 U(\mathbf{x}_s) \, ds \right) \mathbf{e}_i \mathbf{e}_i^\top \right] \\ &= \mathbf{I} + 2v_i \frac{\partial t^*}{\partial \mathbf{x}}^\top \mathbf{e}_i^\top + \frac{2v_i}{\partial_i U(\mathbf{x}^*)} \frac{\partial \mathbf{x}_t}{\partial \mathbf{x}}^\top \left(\int_{t^*}^t \nabla^2 U(\mathbf{x}_s) \, ds \right) \mathbf{e}_i \mathbf{e}_i^\top \end{aligned} \quad (\text{S12})$$

and that

$$\begin{aligned} \frac{\partial \mathbf{p}_t}{\partial \mathbf{x}}^\top \frac{\partial \mathbf{x}_t}{\partial \mathbf{p}} &= \left[\int_0^{t^*} \nabla^2 U(\mathbf{x} + s\mathbf{v}) \, ds + \left(\int_{t^*}^t \nabla^2 U(\mathbf{x}_s) \, ds \right) \frac{\partial \mathbf{x}_t}{\partial \mathbf{x}} \right]^\top \frac{2v_i}{\partial_i U(\mathbf{x}^*)} \mathbf{e}_i \mathbf{e}_i^\top \\ &= 2v_i \frac{\partial t^*}{\partial \mathbf{x}}^\top \mathbf{e}_i^\top + \frac{2v_i}{\partial_i U(\mathbf{x}^*)} \frac{\partial \mathbf{x}_t}{\partial \mathbf{x}}^\top \left(\int_{t^*}^t \nabla^2 U(\mathbf{x}_s) \, ds \right) \mathbf{e}_i \mathbf{e}_i^\top. \end{aligned} \quad (\text{S13})$$

Subtracting (S13) from (S12) yields the identity, completing the proof. \square

LEMMA S1.1. *If $\partial_i U(\mathbf{x} + t^* \text{sign}(\mathbf{p})) \neq 0$, the velocity switch even time t^* as in (4) is a continuously differentiable function of \mathbf{x} and \mathbf{p} with the derivatives*

$$\frac{\partial t^*}{\partial \mathbf{x}} = -\frac{1}{\partial_i U(\mathbf{x}^*)} \mathbf{e}_i^\top \int_0^{t^*} \nabla^2 U(\mathbf{x} + s\mathbf{v}) \, ds, \quad \frac{\partial t^*}{\partial \mathbf{p}} = \frac{1}{\partial_i U(\mathbf{x}^*)} \mathbf{e}_i^\top, \quad (\text{S14})$$

where $\mathbf{x}^* = \mathbf{x} + t^* \mathbf{v}$, $\nabla^2 U$ is the Hessian, and the derivatives are expressed as row vectors.

PROOF. Consider a function $f : \mathbb{R}^{2d+1} \rightarrow \mathbb{R}$ defined as

$$f(t, \mathbf{x}, \mathbf{p}) = |p_i| - \int_0^t \text{sign}(p_i) \partial_i U(\mathbf{x} + s \text{sign}(\mathbf{p})) \, ds.$$

Its derivative with respect to t is given by

$$\partial_t f(t, \mathbf{x}, \mathbf{p}) = -\text{sign}(p_i) \partial_i U(\mathbf{x} + t \text{sign}(\mathbf{p})).$$

Therefore, if $\partial_i U(\mathbf{x} + t^* \text{sign}(\mathbf{p})) \neq 0$, we have $\partial_t f(t^*, \mathbf{x}, \mathbf{p}) \neq 0$ and, by the implicit function theorem (Spivak, 1965), t^* as defined implicitly via (4) is a continuously differentiable function of \mathbf{x} and \mathbf{p} . We now implicitly differentiate (4) in \mathbf{x} and \mathbf{p} , which gives us

$$\begin{aligned} \mathbf{0}^\top &= v_i \partial_i U(\mathbf{x} + t^* \mathbf{v}) \frac{\partial t^*}{\partial \mathbf{x}} + \int_0^{t^*} v_i \frac{\partial}{\partial \mathbf{x}} \partial_i U(\mathbf{x} + s \mathbf{v}) \, ds, \\ \text{sign}(p_i) \mathbf{e}_i^\top &= v_i \partial_i U(\mathbf{x} + t^* \mathbf{v}) \frac{\partial t^*}{\partial \mathbf{p}}. \end{aligned}$$

Rearranging terms, we obtain

$$\frac{\partial t^*}{\partial \mathbf{x}} = -\frac{1}{\partial_i U(\mathbf{x} + t^* \mathbf{v})} \int_0^{t^*} \frac{\partial}{\partial \mathbf{x}} \partial_i U(\mathbf{x} + s \mathbf{v}) \, ds, \quad \frac{\partial t^*}{\partial \mathbf{p}} = \frac{1}{\partial_i U(\mathbf{x} + t^* \mathbf{v})} \mathbf{e}_i^\top. \quad \square$$

S2. Choosing base integration time for Zigzag-NUTS

In Section 4.1, we discuss how to automatically tune an integration time for Hamiltonian zigzag via the no-U-turn algorithm. As we mention there, the base integration time $\Delta T = \nu_{\min}^{-1/2}(\Phi) \Delta T_{\text{rel}}$ for $\Delta T_{\text{rel}} = 0.1$ works well in a broad range of problems but is not always optimal. We explain and illustrate this behavior using the posteriors of Section 4.

As discussed in Section 4.3, the compound symmetric posterior has the probability tightly concentrated along the principal component and are otherwise symmetric in all the other directions. Due to this extreme structure, it takes a while even for Hamiltonian zigzag to gain momentum and start traveling along the least constrained direction. In particular, while Hamiltonian zigzag eventually finds its way over a sufficiently long time period, it also undergoes many local U-turns at a shorter time scale (Figure S1). Such local behavior can cause the no-U-turn algorithm to terminate its trajectory simulation prematurely, leading to an integration time that is too small and sub-optimal (Neal, 2012). Since the algorithm checks for U-turns only at discrete time points $t = 2^\ell \Delta T$ for $\ell \geq 0$, however, we can to a reasonable extent prevent premature trajectory terminations in Zigzag-NUTS by choosing ΔT larger than time scales of local U-turns. For this reason, Zigzag-NUTS performs better with the choice $\Delta T_{\text{rel}} > 0.1$ for these compound symmetric posteriors. As seen in Table S1, we observe 4 to 7-fold increase in ESS for the $\rho = 0.9$ case when moving from $\Delta T_{\text{rel}} = 0.1$ to $\Delta T_{\text{rel}} = 1$.

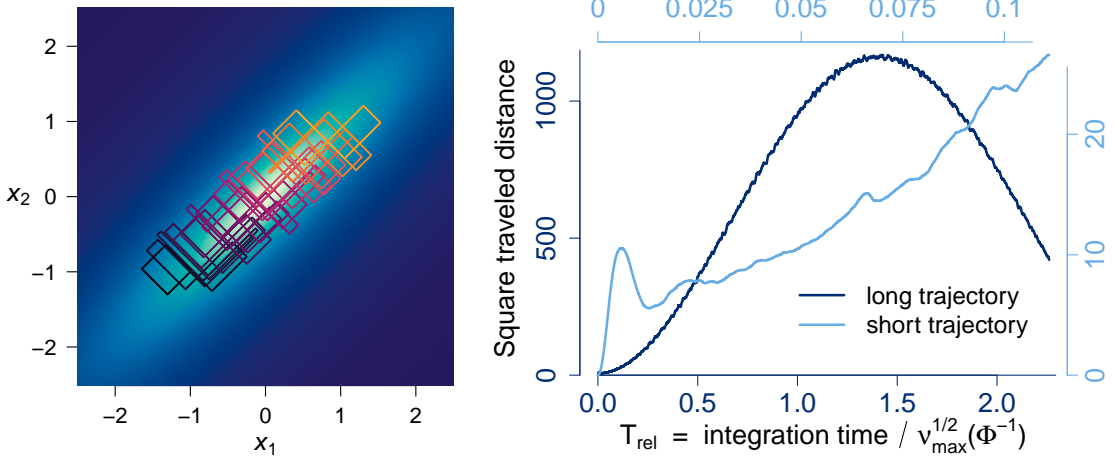


Fig. S1. Trajectory of the first two position coordinates (left) and squared distance $\|x(t) - x_0\|^2$ (right) of Hamiltonian zigzag without momentum refreshment on the 1,024-dimensional truncated compound symmetric target with $\rho = 0.99$. The dynamics is simulated for 4.5×10^5 linear segments, starting from a pre-specified position $x_i = 0.5$ and random momentum $p_i \sim \text{Laplace}(\text{scale} = 1)$. In the left figure, the line segment colors change from darkest to lightest as the dynamics evolves. To the right, the squared traveled distance is plotted as a function of the relative integration time. To help examine the wiggliness at shorter time scales, we zoom into the first 5% of the trajectory and plot it in the lighter blue color.

Table S1. Relative ESS per computing time under the compound symmetric posteriors. The table follows the same format as Table 1 but has additional rows for the results based on Zigzag-NUTS with $\Delta T_{\text{rel}} = 1$.

Compound symmetric	Relative ESS per time			
	$\rho = 0.9$		$\rho = 0.99$	
	x_1	PC	x_1	PC
Case: $d = 256$				
Markovian	1	1	1	1
Zigzag-NUTS ($\Delta T_{\text{rel}} = 0.1$)	4.5	4.6	41	40
Zigzag-NUTS ($\Delta T_{\text{rel}} = 1$)	15	18	55	55
Case: $d = 1,024$				
Zigzag-NUTS ($\Delta T_{\text{rel}} = 0.1$)	4.7	4.5	54	54
Zigzag-NUTS ($\Delta T_{\text{rel}} = 1$)	27	33	78	78

S3. Performance comparison of two zigzags in platform-independent metric

As pointed out in Section 4.2, it is a considerable challenge to account for computational costs of different MCMC algorithms in a practically informative manner. As one alternative to ESS per time, here we consider ESS per velocity switch event as a platform-independent performance metric. This metric is motivated by the similarity in required calculations for the two zigzags’ inter-event simulations (Algorithm 1 and 2). ESS per event is also of theoretical interest since, theoretically speaking, the main difference between the two zigzags arise from the difference in their inter-event time distributions (Line 7 of Algorithm 1 and 2).

In case of truncated Gaussians (Algorithm 3 and 4), our code profiling reveals generating a large number of pseudo-random numbers (Line 7) for Markovian zigzag to be the most computationally expensive step. With the trajectory simulation optimized for truncated Gaussian targets, the rest of the algorithms requires less computational efforts. This fact gives Hamiltonian zigzag an additional advantage in terms of computational speed and hence of ESS per time as presented in Section 4. In contrast, our use of ESS per event here tilts the comparison in favor of Markovian zigzag.

The numerical results of Section 4 are presented, now in terms of the alternative performance metric, in Table S2 and S3. Overall, we observe the same pattern here as in Section 4 — Hamiltonian zigzag outperforms Markovian one except in the i.i.d. Gaussian case, with greater efficiency gain at stronger correlations. The main difference, for the reason we describe above, is that efficiency gains are smaller when measured in ESS per event rather than in ESS per time (cf. Table 1 and 2). We see that relative ESS per time is typically greater than that per event by a factor of 3 to 5.‡

‡ This factor varies more in the i.i.d. Gaussian case (under $\rho = 0$ in Table 1 and S2), ranging from 2.0 — for the case of Zigzag-NUTS ($\Delta T_{\text{rel}} = 0.1$) and $d = 1,024$ — to 8.2 — for the case of Zigzag-HMC and $d = 256$. This greater variations is due to the exceptional simplicity of the i.i.d. Gaussian target; this particular target is so simple that aspects of the algorithms, which ordinarily contribute little to overall computational costs, becomes significant.

Table S2. ESS per velocity switch event — relative to that of Markovian zigzag — under the compound symmetric posteriors. Except for the difference in ESS standardizations, the table follows the same format as Table 1.

Compound symmetric	Relative ESS per event				
	$\rho = 0$		$\rho = 0.9$		$\rho = 0.99$
	x_1	PC	x_1	PC	x_1
Case: $d = 256$					
Markovian	1	1	1	1	1
Zigzag-NUTS ($\Delta T_{\text{rel}} = 0.1$)	0.27	1.2	1.3	8.0	8.0
Zigzag-NUTS ($\Delta T_{\text{rel}} = 1$)	0.37	3.2	3.8	9.6	9.7
Zigzag-HMC ($T_{\text{rel}} = \sqrt{2}$)	0.67	8.3	12	34	34
Case: $d = 1,024$					
Zigzag-NUTS ($\Delta T_{\text{rel}} = 0.1$)	0.29	1.9	1.8	15	15
Zigzag-NUTS ($\Delta T_{\text{rel}} = 1$)	0.33	7.5	9.1	19	19
Zigzag-HMC ($T_{\text{rel}} = \sqrt{2}$)	0.68	16	24	71	71

Table S3. Relative ESS per velocity switch event under the phylogenetic probit posterior. Except for the difference in ESS standardizations, the table follows the same format as Table 2.

Phylogenetic probit	Relative ESS per event	
	min	PC
Markovian	1	1
Zigzag-NUTS ($\Delta T_{\text{rel}} = 0.1$)	2.0	5.9